Bioactive Materials 43 (2025) 32–47

Contents lists available at ScienceDirect

Bioactive Materials

journal homepage: www.keaipublishing.com/en/journals/bioactive-materials

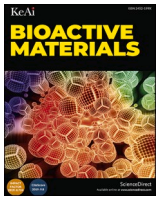

A supramolecular hydrogel leveraging hierarchical multi-strength hydrogen-bonds hinged strategy achieving a striking adhesive-mechanical balance

Jumin Yang [a], Wenguang Liu [a], Wei Wang [a,b,*]

[a] School of Materials Science and Engineering, Tianjin Key Laboratory of Composite and Functional Materials, Tianjin University, Tianjin, 300350, China
[b] College of Chemical and Biological Engineering, Zhejiang University, Hangzhou, 310027, China

ARTICLE INFO

Keywords:
Supramolecular
Tissue-adhesive
Hierarchical multi-strength hydrogen-bonds hinged strategy
Sutureless wound closure

ABSTRACT

To obtain high-performance tissue-adhesive hydrogel embodying excellent mechanical integrity, a supramolecular hydrogel patch is fabricated through in situ copolymerization of a liquid-liquid phase separation precursor composed of self-complementary 2-2-ureido-4-pyrimidone-based monomer and acrylic acid coupled with subsequent corporation of bioactive epigallocatechin gallate. Remarkably, the prepared supramolecular hydrogel leverages hierarchical multi-strength hydrogen-bonds hinged strategy assisted by alkyl-based hydrophobic pockets, broadening the distribution of binding strength of physical junctions, striking a canonical balance between superb mechanical performance and robust adhesive capacity. Ultimately, the fabricated supramolecular hydrogel patch stands out as a high stretchability (1500 %), an excellent tensile strength (2.6 MPa), a superhigh toughness (12.6 MJ m^{-3}), an instant and robust tissue adhesion strength (263.2 kPa for porcine skin), the considerable endurance under cyclic loading and reversible adhesion, a superior burst pressure tolerance (108 kPa) to those of commercially-available tissue sealants, and outstanding anti-swelling behavior. The resultant supramolecular hydrogel patch demonstrates the rapid hemorrhage control within 60 s in liver injury and efficient wound closure and healing effects with alleviated inflammation and reduced scarring in full-thickness skin incision, confirming its medical translation as a promising self-rescue tissue-adhesive patch for hemorrhage prevention and sutureless wound closure.

1. Introduction

Quick establishment of compliant and tough biointerface between bioadhesives and convoluted tissue surface is the key signature of excellent tissue bioadhesive, remaining a challenging task for effective tissue-reconnection owing to wet and dynamic nature of complex physiological environments [1–3]. Synthetic polyacrylic acid (PAAc) and its derivatives, as Food and Drug Administration (FDA)-approved, low-cost, nontoxic polymers with a strong adhesive capacity, have been intensively used as hydrogel matrices for efficient wound closure and rapid hemostatic intervention [4,5]. However, the poor underwater adhesion, unfavorable leakage of body fluid or blood, and prone to secondary tissue damage and scarring, limit its biomedical application in practice [6]. Therefore, it is of great significance to overcome these limitations and improve the functionalities for practically reconnect-internal application of tissue-adhesive hydrogels.

Many researchers have struggled to address excessive hydration and undesirable swelling behavior of PAAc-based hydrogels by means of diverse strategies. Thereinto, it's highlighted that the multilayer design is the most commonly used strategy in current hydrogel design to inhibit excessive swelling [7–9]. Nevertheless, this strategy is generally associated with opaque behaviors, stress concentration, poor interface connectivity, tedious fabrication of multiple procedures and resultantly difficult commercialization promotion and inconvenient application for patients, etc. [10] Therefore, it is ideal to construct monolayer and homogeneous hydrogel systems with limited swelling ability without involvement of laborious preparation course and unfavorable components.

Despite promising strides have been made in the development of synthetic PAAc-based hydrogel patches, their practical application is

Peer review under responsibility of KeAi Communications Co., Ltd.
* Corresponding author. College of Chemical and Biological Engineering, Zhejiang University, Hangzhou, 310027, China.
E-mail address: wwgfz@zju.edu.cn (W. Wang).

https://doi.org/10.1016/j.bioactmat.2024.09.014
Received 27 June 2024; Received in revised form 14 August 2024; Accepted 10 September 2024

consistently hindered by the canonical trade-off between mechanical and adhesive performances. Injured area or surface is not static, but maintains in a state of constant deformation under varying strains, such as bulging, jigging, bending and stretching. Without prominent dynamic compliance and bulk strength, PAAc-based hydrogel patches will inevitably accumulate concentrated stress during the repetitive deformations, thereby incurring eventual interfacial failure [11]. In light of this, the mechanical properties of the PAAc-based hydrogel patches also matter. Dynamic crosslinks based on supramolecular junctions are capable of optimizing the network to impart excellent mechanical integrity of hydrogels and offering functionalities with more diversity and wider spectrums, including surprising tackiness [12–14]. 2-2-Ureido-4-pyrimidone (UPy) is known as self-complementary motif that can dimers by strongly quadruple hydrogen-bonding (H-bonding), which is extensively used in the construction of strong supramolecular network [15,16]. However, due to the rigidity, UPy-based molecules exhibit typically insolubility in water and thus are not suitable for application in hydrogel systems unless emulsion polymerization or organic solvents are utilized [17,18], which is undesirable for the construction of PAAc-based hydrogel patches for biomedical applications. Intriguingly, some macromolecules embodying UPy motifs can undergo liquid-liquid phase separation during the preparation of supramolecular polymers [19], suggesting that this strategy may be used in constructing supramolecular PAAc-based hydrogel driven by strongly quadruple H-bonds to form reinforcing hard domains.

In general, high mechanical performance and robust adhesive capacity are standing at either end of a pair of scales, hardly achieving balance or both, because corresponding cohesive and interfacial adhesion energies are difficult to balance [20,21]. Most reported hydrogels based physical crosslinks have to sacrifice mechanical pursues to realize high adhesive property, or vice versa, hindering their wider application [1,4,6]. Therefore, it is imperative to design PAAc-based hydrogel patches embodying excellent adhesive and mechanical properties simultaneously, further broadening the practical application scopes.

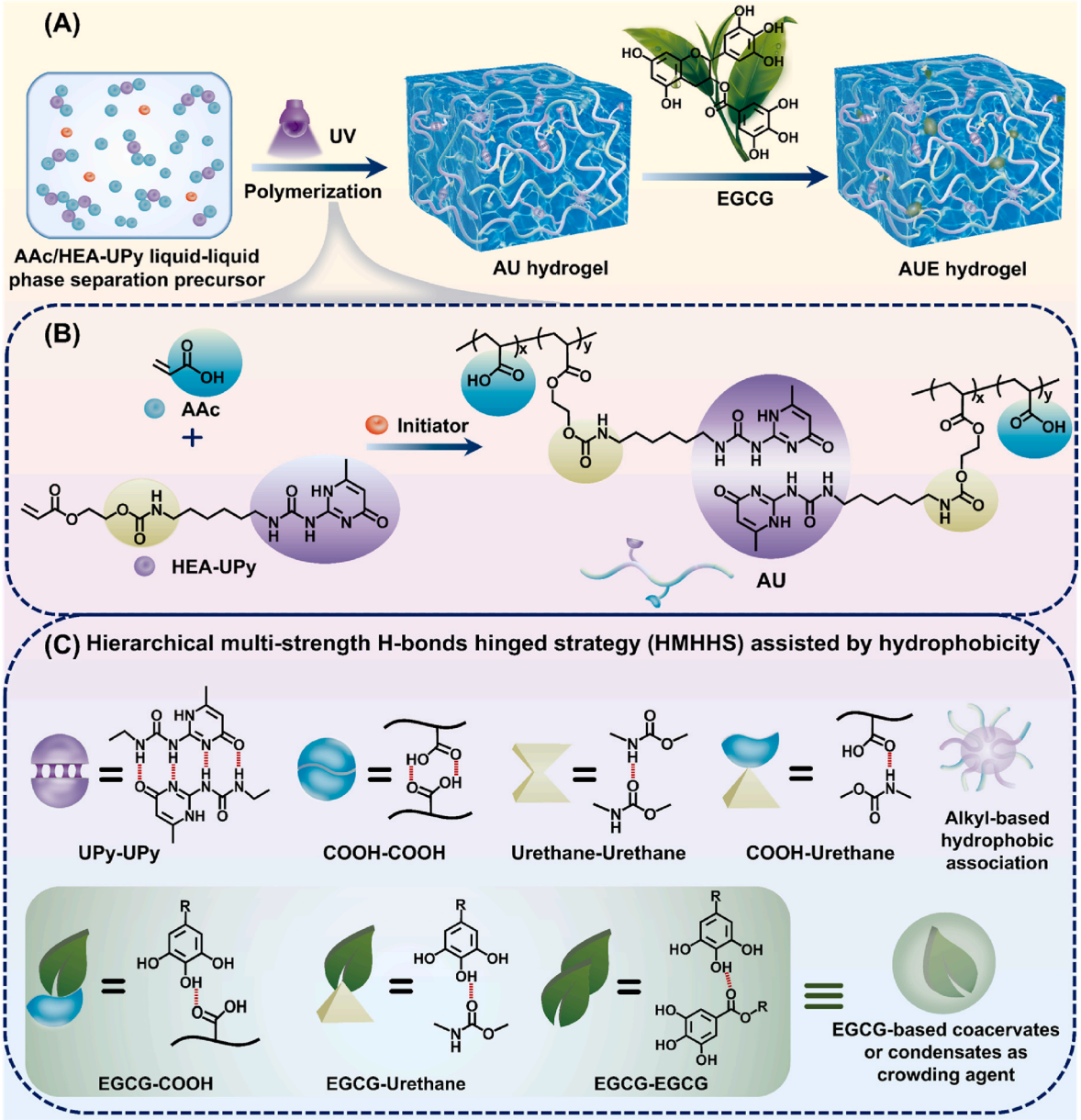

Scheme 1. Schematic illustration of the network formation and composition of supramolecular AUE hydrogels. (**A**) Schematic diagram of the fabricating pathway of AUE hydrogel. (**B**) The molecular structure of supramolecular polymer from AAc/HEA-UPy precursor aqueous solution without involvement of crosslinker and surfactant. (**C**) Schematic illustration of hierarchical multi-strength H-bonds hinged strategy assisted by alkyl-based hydrophobic association.

Inspired by mussel's adhesion, incorporation of catechol-based molecules is promotional in formation of catch bonds under damp environments, and exerting crowding effect via forming coacervates and biomolecular condensates, contributing to robust underwater adhesion [22,23]. Hence, bioactive plant polyphenols emerge as an optimal component for incorporation.

Thus, to develop supramolecular hydrogel patches for efficient wound closure and rapid hemostatic intervention with satisfactory adhesion-mechanical capacity balance and multiple biofunctions, a hierarchical multi-strength H-bonds hinged strategy (HMHHS) is utilized to construct PAAc-based hydrogel network via a one-pot UV-induced copolymerization process, and physical entrapment of epigallocatechin gallate (EGCG) molecules, as displayed in Scheme 1. The prepared supramolecular hydrogel consisting of a copolymer backbone of self-complementary UPy-based monomer and acrylic acid (AAc), and bioactive EGCG-based coacervates, is termed as AUE hydrogel. The hierarchical multiple H-bonding junctions in AUE hydrogel networks include quadruple UPy-UPy H-bonds, double COOH-COOH H-bonds, single urethane-urethane and COOH-urethane H-bonds, and various EGCG-based H-bonds. UPy-based polymer segments can act as actual cross-linker by self-aggregations of strongly quadruple H-bonds assisted by alkyl-based hydrophobic pockets to form reinforcing hard domains, while EGCG can interact with polymer chains via weak H-bonding, forming coacervates or condensates and thus serving as complementary crosslinkers. The hierarchical multiple H-bonds are multi-strength, broadening the distribution of the binding strength of physical junctions, endowing the AUE hydrogel with remarkable properties via synergistic effects. Notably, a canonical balance between superb mechanical performance and robust adhesive capacity can be achieved. The rapid hemorrhage control and effective wound closure and healing are further demonstrated, providing an insight for biomedical applications as self-rescue tissue-adhesive patches with high operability. Overall, this supramolecular hydrogel patch leveraging HMHHS is comparably universal and can be utilized to realize wide-window mechanical property and adhesive performance to further broaden the applicable platforms by adjusting networks.

2. Materials and methods

2.1. Materials

Acrylic acid (AAc, 99 %), 2-amino-4-hydroxy-6-methylpyrimidine (UPy, 99 %), 2-hydroxyethyl acrylate (HEA, 96 %), epigallocatechin gallate (EGCG, 98 %, from green tea), 2,2-diphenyl-1-(2,4,6-trinitrophenyl)hydrazyl (DPPH, ≥97 %, HPLC), 2,2′-azino-bis(3-ethylbenzothiazoline-6-sulfonic acid) diammonium salt (ABTS, ≥98 %), potassium persulfate ($K_2S_2O_8$, ≥99 %), and 2-phenyl-4,4,5,5-tetramethylimidazoline-1-oxyl 3-oxide (PTIO, 98 %) were purchased from Aladdin (Shanghai, China). Hexamethylene diisocyanate (HDI, 99 %) and dibutyltin dilaurate (DBTDL, 95 %) were supplied by Tokyo Chemical Industry (Tokyo, Japan). 2-Hydroxy-2-methyl-1-phenyl-1-propanone (IRGACURE 1173, 98 %) and 3 % hydrogen peroxide (H_2O_2) were obtained from Sigma-Aldrich (St. Louis, USA). Porcine Fibrin Sealant kit was purchased from Guangzhou Bioseal Biotech, Co., Ltd. (Guangzhou, China). 3M Vetbond Tissue Adhesive was acquired from Minnesota Mining and Manufacturing Company (Saint Paul, USA). Cell counting Kit-8 (CCK-8) was received from GlpBio (California, USA). All other solvents were analytical reagents from Heowns Biochemical Technologies Co.,Ltd. (Tianjin, China) and utilized without further refinement.

2.2. Synthesis of HEA-UPy monomer

4-(6-(3-(6-Methyl-4-oxo-1,4-dihydropyrimidin-2-yl)ureido) hexylcarbamoyloxy)-ethyl acrylate (HEA-UPy) was synthesized by referring to previous reports [24]. Firstly, 2 (6-isocyanatohexylaminocarbonylamino)-6-methyl-4 [1H] pyrimidinone (UPy-NCO) was prepared according to the procedure reported in the literature [25]. Subsequently, a mixture of UPy-NCO (2.9 g, 10 mmol) and 2-hydroxyethyl acrylate (1.4 g, 12 mmol) were reacted in trichloromethane ($CHCl_3$, 150 mL) in the presence of DBTDL. And then, the mixture was magnetically stirred at 50 °C for 12 h under nitrogen atmosphere. After the reaction, the mixture was cooled down to the room temperature followed by removing residual solids by filtration under pressure and the resulting filtrate was precipitated into acetone twice. The precipitate was finally dried in vacuum overnight and 3.1 g of white product, denoted as HEA-UPy, was obtained with a yield of 76 %.

2.3. Fabrication of hydrogels

The hydrogels were fabricated using the following procedure. Briefly, AAc and HEA-UPy (1, 2, 3, 4 or 5 mol.%, relative to the total monomer molar concentration) were dissolved in deionized (DI) water to form a homogeneous solution (10 M), followed by the addition of photo-initiator IRGACURE 1173 (0.25 mol.% relative to the monomer molar concentration) and stirring thoroughly with the vortex. Subsequently, the mixture was cast into the mold and then the polymerization was performed for 1 h in a crosslink oven. Upon release of the molds, the formed copolymer hydrogels were directly immersed in DI water for 24 h to remove the unreacted small molecules and then added into the EGCG solution (0.5 % w/v) for 6 h followed by soaking in DI water for equilibrium. Ultimately, the obtained hydrogels were named as AUE-x (x = 1, 2, 3, 4, 5), where x represented the molar percentage of HEA-UPy monomer. Similarly, AU-x (x = 1, 2, 3, 4, 5) hydrogels were prepared as controls by the same protocol except that the step of soaking in EGCG solution was eliminated. Meanwhile, AHE-3 hydrogel was prepared with HEA instead of HEA-UPy as the control by following the same procedures. All freshly prepared hydrogels were used directly without further processing.

2.4. Mechanical tests

The mechanical performances of hydrogels at ambient temperature were investigated by a Legend 2344 electromechanical dynamometer (Instron, USA). All specimens were deformed at an extension rate of 50 mm min^{-1} for tensile test and compression rate of 10 mm min^{-1} for compression test, unless otherwise noted. The cyclic tensile tests were carried out in a water bath at room temperature and the same extension rate was chosen for loading and unloading. For the tensile test, all specimens were cut into normalized dumbbell shapes with a dimension of 50 mm × 4 mm × 1 mm by the punching machine. The Young's modulus was calculated as the slope of the initial linear stage, and the toughness was determined as the area of the tensile curve. At least four parallel samples were measured for each property.

2.5. In vitro adhesion tests

Diverse adhesive substrates including biological tissues and engineering solids were selected for adhesion experiments, and the adhesive strength of hydrogels samples were evaluated via a lap-shear test (ASTM F2255) performed on the same electromechanical tester mentioned above. Hydrogel samples (10 mm × 10 mm × 1 mm) at ambient temperature were sandwiched as interlayer between rectangular substrates with a bonding area of 10 mm × 10 mm. The adhesion strength was determined by the maximum load divided by the joint area. Specifically, porcine skin was selected for simulating adhesion to soft tissue. Lap shear tests were conducted directly after the substrates were bonded with the hydrogel samples to acquire the instant adhesion strength, unless otherwise noted. And underwater adhesion was carried out after the hydrogel-adhered porcine skin tissue were immersed in DI water or highly humid environment for certain time. All experiments were carried out using at least 4 parallel samples.

Furthermore, cyclic tensile lap-shear tests were conducted to assess the adhesive's repeatable adhesion to wet pig skin substrates. The tensile speed was set to 50 mm min^{-1} and the strain was controlled to be 50 %. At least 1000 cycles of adhesion tests were conducted. Moreover, to evaluate the firmness of adhesion, various substrates were glued with hydrogel samples followed by lifting materials substrate and even supporting the weight and the optical images were captured.

2.6. Calculation of binding energy

The binding energy of multiple H-bonds between various donors and acceptors in the AUE-3 hydrogel structures was calculated via the density functional theory (DFT) simulations carried out with the Dmol3 package in Materials Studio with the generalized gradient approximation with Perdew-Burke-Ernzerhof exchange correlation [26]. The convergence criterion for the energy and maximum force for the optimization were set to 10^{-5} Ha and 0.004 Ha/Å, respectively. With the optimized structure, the H-bonding interaction energy was defined as: $E_{binding} = E_{total} - E_{component}$, where E_{total} and $E_{component}$ were the total energy of the system and the energy of each component in the model, respectively.

2.7. Molecular dynamics (MD) simulation test of AUE hydrogel

To compare the structural stability of AUE-3 and AU-3 system, two periodic model cells (AUE-3 and AU-3 hydrogels) containing four random AU copolymer chains (30 repeating AAc units and one random HEA-UPy unit), 12 EGCG molecules (without EGCG molecules in AU-3 system) and 180 water molecules were constructed by randomly distributing the polymer chains in the cubic box in the Amorphous Cell module of the Materials Studio, in which the initial density of the polymer is set to be 0.5 g cm^{-3} [27]. The structure optimization and the calculation of the cohesive density and H-bonds were performed in the Forcite module of Materials Studio software. The COMPASS (condensed-phase optimized molecular potentials for atomistic simulation studies) III forcefield was utilized to describe the atomic interactions in both systems, while the partial atom charges were assigned using the method of Gasteiger.

2.8. In vitro burst pressure quantification

Burst pressure test was carried out using a home-designed setup as previous reports [6]. In brief, a segment of porcine small intestine was cut and filled with PBS solutions to mimic the humid surface environment. Then, the porcine small intestine was fixed to a home-designed device linked to a syringe pump and a digital pressure gauge through a three-way stopcock. A 3-mm-diameter hole was created on the surface of the intestine. Subsequently, the AUE hydrogel samples with a diameter of 8 mm and a thickness of 0.5 mm were applied to seal the hole. The peak pressure observed on the screen of the digital pressure gauge was determined as the burst pressure throughout the PBS pumping process (2 mL min^{-1}). Commercially available bioadhesives, Fibrin and Vetbond glue, were selected as controls and measured by injecting 200 μL following the same parameters and conditions. All measurements were repeated five times for each group.

2.9. In vivo hemostatic test

In vivo hemostatic tests were performed on the liver of Sprague-Durer (SD) rats (male, 250 ± 30 g in weight). Prior to the operation, the rats were anticoagulated by intraperitoneal injection of heparin (3000 U/kg), followed by anesthetization with pentobarbital sodium and fixation on the operating board. Subsequently, the livers were exposed through an abdominal incision. The blood on the surface of the liver was wiped away and a piece of filter paper was placed under the liver to absorb the blood from the wound. For the rat liver trauma model, the liver was punctured with a 26-G needle. And for the rat liver linear incision model, an incision of 10 mm in length and 5 mm in depth was created on the lobe of the liver with a surgical scalpel. The AUE hydrogel was immediately applied to the bleeding site to seal the wound. No treatment was carried out for the control group. To assess the hemostatic capacity, the whole process was captured with a camera, and meanwhile the time to hemostasis was recorded. At last, the blood loss was calculated by comparing the weight of filter paper before and after the tests. All measurements were performed with four repetitions.

2.10. In vivo wound closure and healing tests

The hydrogel wound closure and healing performance were assessed in a full-thickness skin incision model using 12 SD rats (male, 250 ± 30 g in weight). After anesthetization with pentobarbital sodium, the back hair of the rats was removed followed by disinfection with povidone-iodine. A full-thickness skin incision of 2 cm was created on the dorsal skin of each rat with a surgical scalpel. The AUE hydrogel strip (30 mm × 10 mm × 1 mm) was applied to the incisions to seal the wound. For comparison, the incisions were treated with PBS and conventional suture. The wound closure effect was observed with a digital camera on day 1, 3 and 7 post-operation. The rats were euthanized 7 days after the operation, and the skin around the wounds was harvested for histological assessments. On the basis of hematoxylin and eosin (H&E) staining images, the mean wound length of the epidermis and dermis were calculated via the ImageJ software. All measurements were performed by analysts blinded to the tested groups.

2.11. Statistical analysis

Experimental data were presented as means ± standard deviations (SD). GraphPad Prism 9.0 was used for statistical analysis of data. Statistical analysis was performed using Students' t-test for two-sample analyses and one-way analysis of variance (ANOVA) followed by post hoc Bonferroni test for multiple sample analyses to calculate the P values. $^{*}P < 0.05$, $^{**}P < 0.01$, $^{***}P < 0.001$ were identified as statistical significance and *ns* represented no significance.

3. Results and discussion

3.1. Synthesis of AUE hydrogel

Firstly, an intriguing monomer HEA-UPy composed of an acrylic head, a hydrophobic alkyl spacer linked by carbamate, and a UPy motif as tail [16], to generate abundant hydrophobic association and H-bonds simultaneously, was synthesized as previously reported method as illustrated in Fig. S1 (Supporting **Information**). The chemical structure of HEA-UPy was determined by ^{1}H nuclear magnetic resonance (^{1}H NMR) and exhibited in Fig. S2 (Supporting **Information**).

Molecules based UPy motif are extensively devoted to preparing supramolecular materials with promising properties, while excruciating hydrophobic nature is endowed by hydrophobic alkyl spacer and rigid UPy units, resulting in strongly incompatibility with water and necessary involvement of toxic surfactants for emulsion polymerization [24]. A fascinating phenomenon known as liquid-liquid phase separation occurs in AAc/HEA-UPy aqueous solution systems likely due to their cosolvency in water boosted by interactions between AAc and HEA-UPy, reminiscent of deep eutectic solvents with enhanced solubility derived from strong H-bonding [27,28]. Consequently, AAc/HEA-UPy precursor solution undergoes in situ copolymerization with the existence of photo-initiator IRGACURE 1173, affording a supramolecular hydrogel driven by multiple H-bonding clusters and hydrophobic effects. Notably, the polymerization process is rather simple and eco-friendly without the involvement of troublesome emulsification systems and additional chemical crosslinkers. The synthetic supramolecular hydrogels are denoted as AU-x (x indicates the molar percentage of HEA-UPy). A series

of AU hydrogels with incremental densities of HEA-UPy from 1 mol.% to 5 mol.% at a constant total monomer content were fabricated. Notably, larger molar ratio of UPy units (> 5 mol.%) is not considered in this work due to the increasing insoluble systems. In AU hydrogel systems, HEA-UPy not only acts as a reactive monomer, but also plays a pivotal role as actual cross-linker to accelerate the formation of associative networks.

However, reduced elasticity ascribed to abundant hydrophobicity-assisted strong quadruple H-bonding clusters with relatively low reversible kinetics, and the intrinsically weak wet adhesion of PAAc, would inevitably limit its further application in challenging hemostasis scenarios [4,23]. To address those issues, a facile method inspired by the crowding effect and mussel's adhesion matrix was developed to tune supramolecular H-bonding networks [23,29]. Subsequently, EGCG molecules, the dominant components of green tea polyphenols, were selected and incorporated via a simple mixing process with associative AU polymers after polymerization, affording AUE-x hydrogels (x represents the molar percentage of HEA-UPy). EGCG molecules can interact with AU polymers and themselves via various weak H-bonding and π-π stacking, causing the coacervates or aggregations of EGCG molecules in polymer chains and thus serving as biomolecular crowding agents and complementary crosslinkers [30]. From the dynamics perspective, the

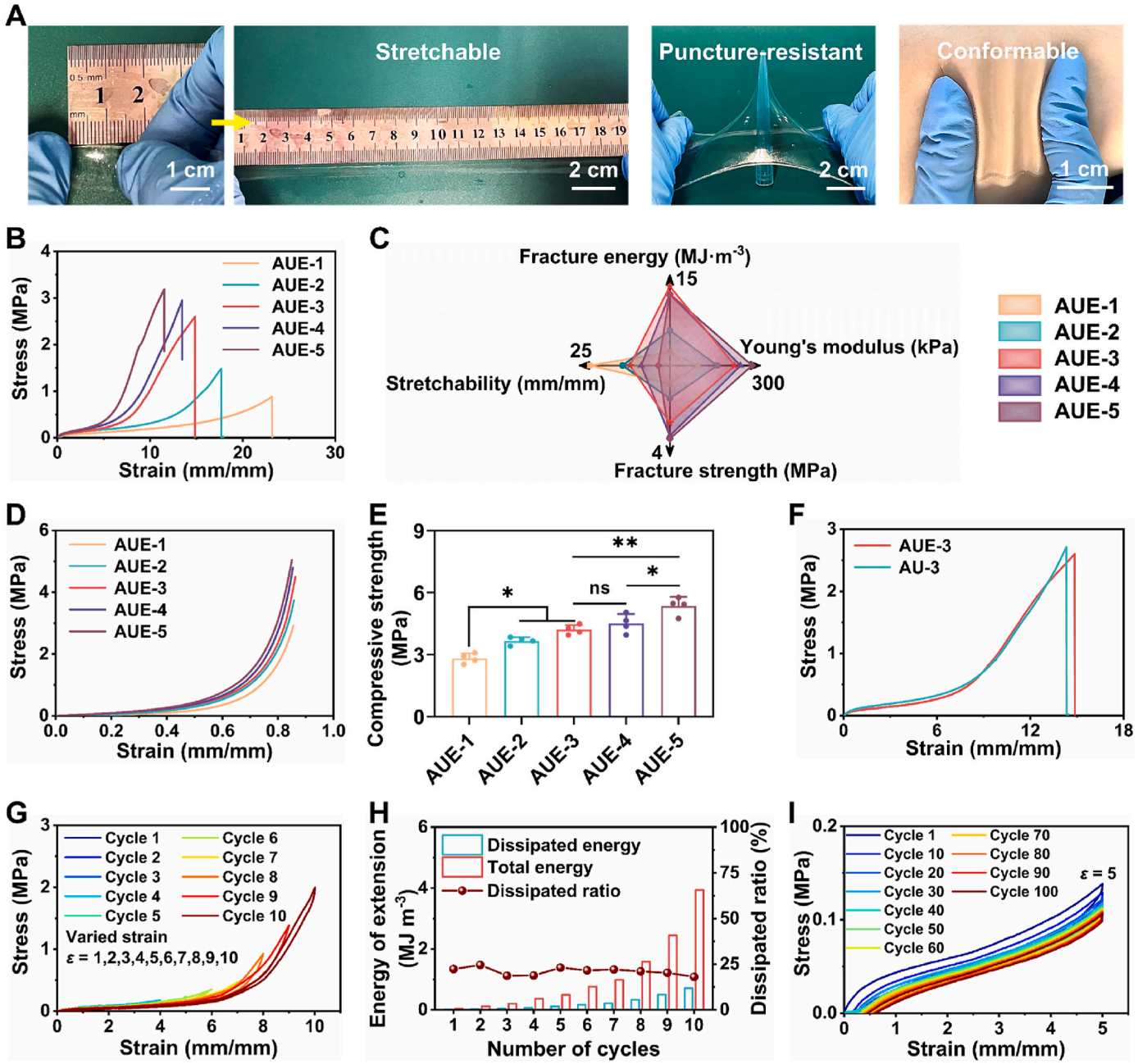

Fig. 1. Mechanical performances of AUE hydrogels. (**A**) Digital photographs illustrating the appearance and mechanical performances of AUE-3 hydrogel. (**B**) Tensile stress-strain curves of AUE hydrogels. (**C**) Corresponding comparison of AUE hydrogels in respect to fracture energy, Young's modulus, fracture strength and stretchability. (**D**) Compressive stress-strain curves of AUE hydrogels. (**E**) Corresponding compressive strength of AUE hydrogels. Data are expressed as mean ± SD. The significant difference was detected by one-way ANOVA. n = 4, $^{*}P < 0.05$, $^{**}P < 0.01$ and ns: no significance. (**F**) Tensile stress-strain curves of AUE-3 and AU-3 hydrogels. (**G**) Sequential loading-unloading tensile curves of AUE-3 hydrogel without pausing between each cycle under different strains (ε = 1–10). (**H**) Corresponding calculated total and dissipated energy and dissipated ratios of AUE-3 hydrogel. (**I**) Cyclic tensile stress-strain curves of AUE-3 hydrogel at a constant strain of 5 for uninterrupted 100 cycles.

pyrogallol/catechol groups of these bioactive crowding agents preferentially seize free COOH and urethane motifs to form weak H-bonds to increase H-bonds density of associative polymer networks, buffering the rigidity of network endowed by the hard quadruple H-bonding-clusters domains. Thus, enhanced weak H-bonds density and attenuated rigidity of the network can be conductive to the folding and entanglement of polymer chains, further promoting the maximization of the entropy of networks and strengthening the entropic elasticity and conformational resilience [11,31]. Moreover, polyphenol-network-mediated surface chemistry further propels the wet adhesion of obtained hydrogels. Ultimately, such a hierarchical multi-strength physical crosslinked strategy can greatly broaden the distribution of the binding strength of H-bonding junctions [32].

The chemical structures of as-obtained AUE hydrogel were confirmed by attenuated total reflection fourier transform infrared (ATR-FTIR) spectroscopy (Fig. S3, Supporting **Information**). Moreover, as observed in the scanning electron microscopy (SEM) images (Fig. S4, Supporting **Information**), AUE hydrogel with EGCG demonstrates the smallest pores compared to AU hydrogel, indicating a higher density of such hierarchical multiple H-bonding junctions.

3.2. Mechanical and self-healable performances of the AUE hydrogels

As displayed in Fig. 1A, the fabricated AUE-3 hydrogel is transparent, flexible, stretchable, conformable and puncture-resistant. The AUE-3 hydrogel can endure various deformations, such as stretching more than 1500 % without observable rupture, resisting the puncture of 1 mL gun tip and fitting well on the uneven skin surface. By tracking the amount of UPy moiety in AUE hydrogels and whether EGCG was involved or not, the systematically mechanical process in real time was followed. As displayed in Fig. 1B, the more UPy-based fragment, the closer the tensile stress-strain curves of AUE hydrogels are observed to be the J-shaped curve with strain-stiffening character [33]. The corresponding tensile performances as fracture strength, Young's modulus, stretchability and fracture toughness are shown in Fig. 1C. All AUE hydrogels are highly stretchable, from 1160 % of AUE-5 hydrogel to 2320 % of AUE-1 hydrogel. As the amount of UPy in hydrogels increases, the tensile stress required to stretch increases systematically. It is also noted that the 3 mol.% content of UPy-based unit reaches a critical value. The fracture strength, Young's modulus and fracture toughness of AUE hydrogels below 3 mol.% content of UPy-based unit are relatively low, while those of hydrogels above 3 mol.% are merely a little higher but the stretchability significantly diminishes. Furthermore, as shown in Fig. S5 (Supporting **Information**), the tensile stress-strain curve of AHE-3 hydrogel is nearly negligible compared with that of AUE-3 hydrogel, and their mechanical properties are not of the same order of magnitude. The corresponding fracture energy, Young's modulus, tensile strength and stretchability of AUE-3 hydrogel are significantly higher than those of AHE-3 hydrogel due to the absence of UPy moiety to form hardening quadruple H-bonding crosslinks and resultant loose hydrogel network and high swelling property. The schematic diagram of dynamic bond breakage in AUE-3 hydrogel during the stretching process was presented in Fig. S6 (Supporting **Information**), suggesting that its excellent tensile performances can be ascribed to the gradually breakage/reconstruction of multiple physical crosslinks in response to loading in AUE hydrogels. Hence, with increasing UPy content, the density of load-bearing UPy dimers assisted by alkyl-based hydrophobic pockets is accordingly higher, which will accumulate into nano-sized and hydrophobic phase separation domains (the cluster and stacks of quadruple H-bonding) to self-reinforce the hydrogel. Combining COOH-COOH H-bonding clusters, urethane-urethane H-bonding crosslinks and EGCG-based noncovalent crosslinks (H-bonds predominate) contributes to a tremendous increase in the tensile mechanical property. However, too high density of UPy-based fragments enables supramolecular polymer chains close to semi-rigidity, leading to a decrease in the toughness and stretchability of hydrogels. Specifically, AUE-3 hydrogel demonstrates the optimized mechanical performances, including an impressive extensibility of 1500 % ± 88 %, an ultimate stress of 2.6 ± 0.2 MPa, a Young's modulus of 181.2 ± 14.0 kPa and a superhigh facture energy of 12.6 ± 1.1 MJ m^{-3}. Similarly, the increment in the compressive performances of AUE hydrogels is in full agreement with the increased content of UPy-based unit, as shown in Fig. 1D and **E**. In conclusion, the self-reinforced behavior via hydrophobicity-assisted hierarchical multiple H-bonding structure endows the prepared AUE hydrogel with excellent mechanical properties (high tensile strain, strength and toughness), which is conductive to maintaining mechanical integrity and preventing material damage under loading.

The AUE-3 hydrogel demonstrates the optimized toughness with high elongation, and thus is selected for further study to evaluate the effect of EGCG on mechanical performances with AU-3 hydrogel as control. As observed in Fig. 1F and Fig. S7A, **B** (Supporting **Information**), the tensile and compressive strengths of AUE-3 hydrogel are not significantly different from those of AU-3 hydrogel, verifying that the alternative crowding effect of EGCG can compensate for enhanced effects of some restricted strong H-bonding clusters. Minimizing energy dissipation is crucial for high-performance hydrogels that require repetitive actions [34]. Energy dissipation of AUE-3 and AU-3 hydrogels were investigated by means of continuous cyclic tensile loading under diverse stretching ratios. As displayed in Fig. S7C, **D** (Supporting **Information**), as the tensile strain aggrandizes from 1 to 10 without interval, the dissipation energy of AU-3 hydrogel with obvious hysteresis loops increases from 0.02 to 1.6 MJ m^{-3}, and the corresponding dissipated ratios are relatively high (~ 31 %), indicating the efficient energy dissipation of AU-3 hydrogel toughened by strongly H-bonding clusters including COOH-based H-bonding clusters and UPy-based quadruple H-bonding clusters. In stark contrast, as demonstrated in Fig. 1G and **H**, AUE-3 hydrogel exhibits no apparent mechanical hysteresis during successive loading-unloading process under different strains ($\varepsilon = 1$–10). The dissipation energy of AUE-3 hydrogel is gradually enhanced from 0.01 to 0.7 MJ m^{-3} when the strain augments step by step to 10, and the corresponding dissipation ratios are rather low (20 %), indicating good elasticity and high reversibility at various deformations. This remarkable mechanical behavior was further corroborated by cyclic tensile tests at a strain of 500 %. As shown in Fig. 1I and Fig. S7E (Supporting **Information**), the cyclic tensile curves of AUE-3 hydrogel are basically invariant even after 100 cycles, maintaining a low hysteresis loop, while the AU-3 hydrogel cannot withstand cyclic tensile loading over 20 cycles without no deterioration at a high strain of 5 and its cyclic tensile curves are apparently different after 10 cycles, signifying lower reversibility in a short time. The lower reversibility of AU-3 hydrogel can be attributed to partial polymer chain fracture due to the difficulty of recovering strong UPy-based dimeric H-bonding clusters [35]. Based on the elastic performance of AUE and AU hydrogels, it is clear that EGCG matters for retraction process of AUE-3 hydrogel, which might be ascribed to two reasons [36]. On the one hand, the EGCG containing pyrogallol/catechol groups preferentially forms weak H-bonds with free COOH and urethane groups in polymer chains to increase weak H-bonds density, contributing to preventing slippage of polymer strand segments through dense H-bonding crosslinking points [37]. Due to the metastable and dynamic nature during the stretched state, these weak noncovalent bonds can autonomously recover to the initial state when the load is released, while strong UPy dimer-aggregated hard domains take time to be completely reformed, showing a relatively low reversibility and weak dynamics owing to high quadruple H-bond energy and slow mobility of stiff and hydrophobic UPy motifs [36]. On the other hand, EGCG-based H-bonding coacervates as crowding agents promote the folding and entanglement of polymer chains and the maximization of the entropy of networks [11,31]. During stretching, partial energy can be dissipated based on entropy loss, leading to a high reversibility and entropic elasticity under load [38]. Ultimately, combining the synergistic effects endowed by hierarchical multi-strength (quadruple, double and single) H-bonding clusters and aggregations coupled with alkyl-based

hydrophobic pockets, AUE-3 hydrogel reconciles the typical trade-off between a high facture energy and reversibility of energy dissipation structures, that is, achieving both of high toughness and elasticity. Compared with the reported representative hydrogels in recent years [37–39], AUE-3 hydrogel developed in this study displays both superior toughness and low hysteresis in large tensile cycle deformation range, breaking the toughness-elasticity correlation [40,41].

As observed in Fig. S8A (Supporting **Information**), AUE-3 hydrogel exhibits preeminent scar elimination ability. An obvious scar made on the surface of AUE-3 hydrogel strip is observed to nearly vanish from sight after healing for 24 h at 60 °C. Furthermore, AUE-3 hydrogels were cut into two separate pieces and subjected to tensile stress-strain tests after different restoration time at 60 °C. As depicted in Fig. S8B (Supporting **Information**), within the different healing time, the healed AUE-3 hydrogel displays approximately coincident tensile stress-strain curves as the pristine one expect for failure at diverse elongation ratios, demonstrating time-dependent healing efficiency. Notably, the healed AUE-3 hydrogel maintains an elongation of ~1200 % and a stress of ~1.2 MPa (Fig. S8C, Supporting **Information**), suggesting a tolerable self-healing efficiency and mechanical strength. Mechanistically, the self-healing performance is likely to derive from the dynamic reversibility of its hierarchical multiple physical crosslinks. Given the well-defined supramolecular interactions in AUE-3 hydrogel, the multiple H-bonds are multi-strength, presenting as a strength order of quadruple (UPy motif) **>** double (COOH) **>** single (urethane and EGCG) [36]. When hydrogel cuts are in close proximity to each other, different degrees of reorganization of multi-strength H-bonds can occur. The easily mobile units including COOH, urethane and EGCG preferentially reform weak H-bonds with lower energy and rapid dynamics. In comparison, the strong UPy dimers take times to be completely reconstructed, showing relatively weak dynamic reversibility derived from high quadruple H-bonding energy and slow movement of rigid and hydrophobic UPy units. The preferential restructuring of weak H-bonds may occupy the active sites of strongly UPy dimeric H-bonding reassembling, leading to attenuated tensile strength of the healed hydrogel [42].

3.3. Adhesion performances of AUE hydrogels

Firm tissue adhesion of hydrogels is prerequisite for intimately contacting wet tissues for seamlessly wound hemostasis and closure [6]. To quantitatively evaluate the adhesion performance, standard lap-shear tests on various tissues or engineering solids were conducted to measure the shear strength of hydrogels as displayed in Fig. 2A. Porcine skins were selected as representative wet tissues to determine the instantly adhesion strength of AUE hydrogels in air with varying UPy-based segment contents and AHE-3 hydrogel without UPy moiety. As detected in Fig. 2B and **C**, the instantly shear strength of AUE hydrogels are enhanced initially to reach the highest value (263.2 ± 12.6 kPa) in AUE-3 hydrogel and then decreases with higher UPy motifs contents. This is attributed to the promotional effects endowed by alkyl-assisted UPy-based segments that can establish hydrophobic and quadruple H-bonding junctions and prevent electrostatic repulsion of PAAc chains simultaneously [4,25]. However, too high content of UPy-based segments is detrimental to robust adhesion likely due to excessive bulk strength and reduced flexibility and a resultant improved cohesive energy exceeding the adhesion energy [43]. Significantly, the adhesion capacity of AHE-3 without UPy moiety is much lower than those of AUE hydrogels, and its adhesion strength for porcine skins is merely 21.8 ± 3.9 kPa, indicating the indispensable role of UPy moiety in AUE hydrogels on adhesion performance. Accounting for adhesion strength and mechanical strength, AUE-3 hydrogel was selected as the finally and optimal recipe and used in this study. Notably, AUE-3 hydrogel exhibits tough and durable underwater adhesion in diverse wet environments as well (Fig. 2D and **E**). Immersing in water for 12 h (W-12 h) and displacement in highly humidity condition for 24 h (H-24 h) merely cause no significant decrease of adhesion strength. Despite immersing in water for 24 h (W-24 h), it still maintains strongly adhesive to porcine skins with an adhesion strength of 182.4 ± 29.1 kPa, which is remarkably higher than the instant adhesion strengths of commercially-available bioadhesives (Fibrin sealant and Vetbond) and some typical reported PAAc-based adhesives in air [4,22,44].

In addition to porcine skins, AUE-3 hydrogel also demonstrates benign and comparable adhesive capacity for multiple biological tissues and engineering solids. As shown in Fig. 2F, the adhesive strengths of AUE-3 hydrogel towards smooth porcine stomach and heart are 114.1 ± 8.7 kPa and 69.7 ± 12.6 kPa, surpassing previous reported hydrogel adhesives [45–47]. Meanwhile, AUE-3 hydrogel could also be successfully adhered to all kinds of engineering solid surfaces with varying shear strengths ranging from 574.7 ± 57.2 kPa for wood to 26.8 ± 7.9 kPa for notoriously non-stick poly (tetrafluoroethylene) (PTFE). Furthermore, our AUE-3 hydrogel exhibits saliently higher adhesive performances for almost all substrates than those of AU-3 hydrogel, presumably derived from the formation of interfacial interactions with substrates donated by pyrogallol/catechol groups of the EGCG, which include H-bonding, metal coordination, π-π/cation-π interactions, and hydrophobic interactions [22,48]. As vividly displayed in Fig. 2G, photographs of AUE-3 hydrogel adhering to diverse substrates were obtained. Specifically, AUE-3 hydrogel possesses the faculty to close artificial wounds of porcine organs and support its own weight. Remarkably, broken small intestine and colon can be effectively sealed by AUE-3 hydrogel patch following bearing perfusion of tap water without any leakage, highlighting its rapid and tough adhesion in a wet environment. Therefore, AUE-3 hydrogel overcomes the canonical contradiction between superb mechanical performances and robust adhesive capacity, with mechanical properties (high tensile strength, stretchability and toughness simultaneously) and adhesive strength for exceeding those already reported adhesive hydrogels (Fig. 2H and Table S1, Supporting **Information**). Above results confirm that the precise coordination of supramolecular network and polyphenol-mediated surface chemistry enables AUE-3 hydrogel to establish rapid and robust wet adhesion as satisfactory bioadhesive patch, suggesting its potential application in sweaty and aquatic environments.

Furthermore, a cyclic tensile lap-shear test within 50 % strain by sandwiching hydrogel materials between two porcine skins was performed to evaluate the dynamic adhesion performance over time as uncovered in Fig. 2I. Apparently, AUE-3 hydrogel demonstrates a strong and repeatable adhesion on porcine skins, as evidenced by a well sustaining after 1000 cycles of lap-shearing deformations without any obvious decay. At the same time, AUE-3 hydrogel can seal the needle hole of the punctured ballon to endure repeated deflation-inflation cycles (Fig. S9 and **Video S1**, Supporting **Information**), indicating firmly dynamic adhesion and excellent conformability of AUE-3 hydrogel. This distinct dynamic adhesive capacity is likely attributed to two aspects. On the one hand, hierarchical multiple reversible interactions between AUE-3 hydrogel and skin surface endow the hydrogel with immediate and repeatable adhesion [49]. On the other hand, its rapid self-recoverability demonstrated by cycle loading-unloading tests is beneficial to satisfactory reusability in adhesion [50].

Generally, tightly bound interfacial water layer on tissue surfaces effectively hinders intimate contact between hydrogels and tissues, and a majority of reported wet-adhesive hydrogels based on PAAc have extremely high swelling ratios, incurring severe weakening of wet-adhesive strength [44,51]. In a wet environment, an appropriate swelling profile can be crucial in achieving durable and reliable tissue adhesion for the hydrogel [52]. As shown in Fig. S10A, compared with AUE-1 and AUE-2 hydrogels, AUE-3 hydrogel exhibits a stable swelling kinetic, indicating that the interfacial drainage effect enhanced by strongly hydrophobicity-assisted UPy-UPy aggregations and stacks. Even after soaking in water for 14 days, AUE-3 hydrogel maintains similar swelling area as original state (Figure S10B, Supporting **Information**), and this excellent swelling outcome is principally attributed to

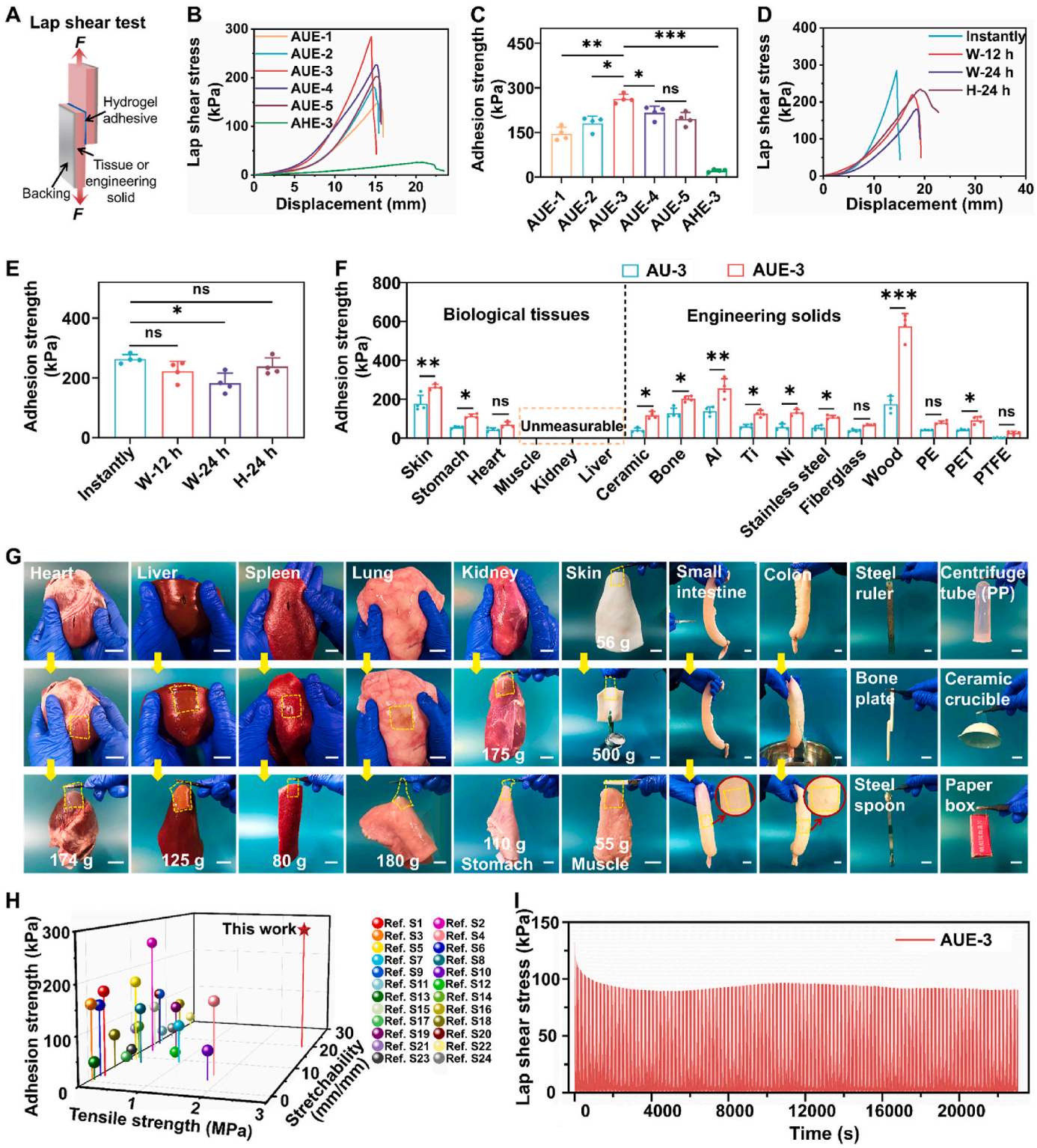

Fig. 2. Adhesion performances of AUE hydrogels. (**A**) Schematic illustration of the lap shear test. (**B**) Typical lap shear stress-displacement curves for wet porcine skins adhered by AUE hydrogels with varying UPy moiety contents and AHE-3 hydrogel without UPy moiety. (**C**) Adhesion strength between porcine skin and AUE hydrogels with varying UPy moiety contents and AHE-3 hydrogel without UPy moiety. (**D**) Typical lap shear stress-displacement curves for wet porcine skins adhered by AUE-3 hydrogel under different wet environments. (**E**) Adhesion strength between porcine skin and AUE-3 hydrogel under different wet environments. (**F**) Adhesion strengths of AUE-3 and AU-3 hydrogels for different substrates. (**G**) Digital photographs of adhesive performance of AUE-3 hydrogel on various substrates. The yellow dash lines indicate hydrogel edges. Scale bar: 20 mm. (**H**) Comparison of this work with previous reported tough and adhesive hydrogels in terms of tensile strength, stretchability and adhesiveness. (**I**) Lap shear stress curve of AUE-3 hydrogel to wet porcine skin subjected to 50 % tensile strain over 1000 loading-unloading cycles. Data are expressed as mean ± SD. The significant difference was detected by one-way ANOVA. n = 4 for (**C**, **E**, **F**), $^{*}P < 0.05$, $^{**}P < 0.01$, $^{***}P < 0.001$ and ns: no significance.

the strongly self-aggregations of alkyl-based hydrophobic pockets and multiple H-bonding clusters donated by UPy-based segments and EGCG-based coacervates, which are capable of helping destroy the hydrated layer on the substrates and resisting undesirable electrostatic repulsion of PAAc chains, thus preventing excessive swelling [1]. The swelling-tolerant capacity of AUE-3 hydrogel is conductive to establishing a long-lasting and reliable adhesion immediately in a wet environment.

3.4. Internal interactions in AUE hydrogel

It is highlighted that one frequently utilized hydrophilic unit coupled with a self-complementary UPy unit to construct synthesized supramolecular systems is a controllably water-soluble system without additional toxic surfactants and chemical crosslinker. To further evidence the presence of the supramolecular network, the dynamic light scattering (DLS) analyses of AAc/HEA-UPy (AU) precursor solutions with varying UPy moiety content and AAc aqueous solution were performed. As displayed in Fig. 3A, no obvious peak in pure AAc aqueous solution is observed, suggesting homogeneous solution formation. Whereas, there are apparent peaks at 5–10 nm in the AU precursor solutions, and the increase in hydrodynamic diameter is ascribed to a higher UPy moiety content. The size of micro phase at 6 nm should arise from hydrophobic association and suppressed UPy-based H-bonding clusters provoked by the disruption of AAc [27]. Intriguingly, the interactions between AAc and HEA-UPy give rise to their cosolvency in

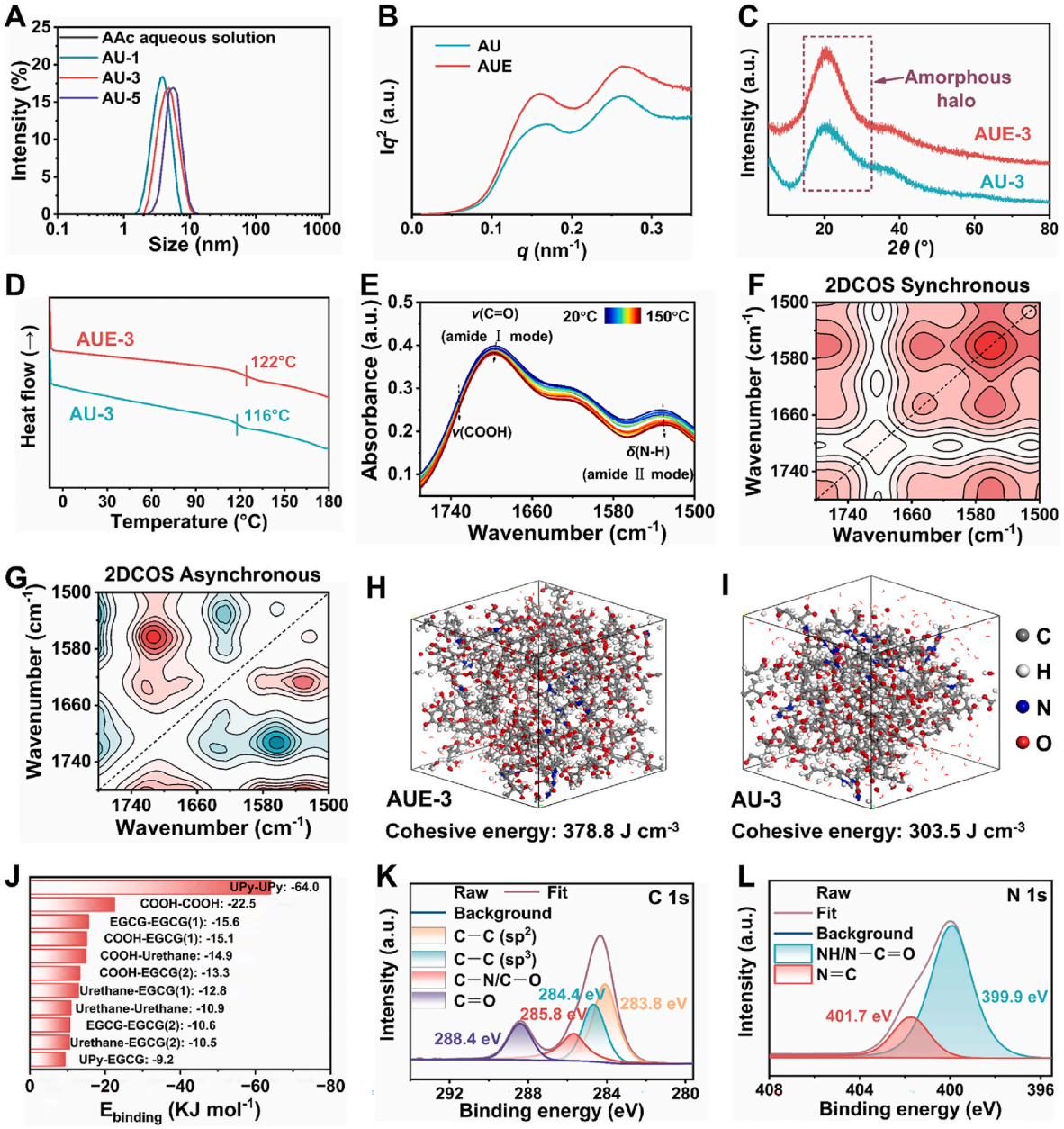

Fig. 3. Internal interactions in AUE hydrogel. (**A**) DLS size distribution curves of AAc aqueous solution and AAc/HEA-UPy precursor solutions with varying UPy moiety contents. (**B**) Iq^2–q profiles of dry AUE-3 and AU-3 hydrogel via SAXS measurements. (**C**) XRD curves of AUE-3 and AU-3 hydrogels. (**D**) DSC curves of AUE-3 and AU-3 hydrogels. (**E**) Temperature-variable FTIR spectra of AUE-3 hydrogel. (**F**) 2DCOS synchronous spectra of AUE-3 hydrogel during heating. (**G**) 2DCOS asynchronous spectra of AUE-3 hydrogel during heating. The red and blue colors represent positive and negative intensities, respectively. (**H**) Snapshot of MD simulation of the structure of AUE-3 hydrogel. (**I**) Snapshot of MD simulation of the structure of the AU-3 hydrogel. (**J**) Binding energy of multiple H-bonds in the AUE-3 system as calculated by DFT. (**K**, **L**) Peak-fitting XPS in the C1s (**K**) and N1s (**L**) regions of the surface of AUE-3 hydrogel. a. u., arbitrary units.

water, leading to a heterogeneous liquid-liquid phase separation solution [23,28]. The resulting solution is transformed into a supramolecular hydrogel upon polymerization, affording phase separation nanostructure largely driven by maximization of the translational entropy in strong H-bonding and hydrophobic effects, followed by the construction of EGCG-based H-bonds [53].

It is noted that previous reports uncovered that multiple H-bonding aggregations bring about the formation of multiphase separation structure [36]. Herein, small-angle X-ray scattering (SAXS) measurements were conducted to study the internal nanostructure of AUE-3 and AU-3 hydrogels. As exhibited in Iq^2-q profiles (Fig. 3B), two clearly broad scattering peaks are detected in AUE-3 and AU-3 hydrogels, verifying a disorganized dispersion of nano-sized microphase separation domain. The scattering peak appearing in the low q regime presumably corresponds to a micro-region size of 39 nm among the dense aggregation and stacks of hydrophobicity-assisted quadruple UPy-based H-bonding clusters, while the other with periodicity calculated as 23 nm is likely driven by the aggregation of COOH-based and urethane-based H-bonding clusters in the supramolecular network. In this case, the aggregation and stacks of hard domains as physical cross-linking sites in networks can exert a promotional effect on the mechanical attributes such as toughness, while soft alkyl spacers can enhance the stretchability and weak H-bonds can be constructive for its self-healing capacity, eventually reconciling the paradox between mechanical strength and self-healing capacity of AUE hydrogels, in accordance with the results in Fig. 1 and Fig. S8 (Supporting **Information**) [26].

In addition, the appearance of merely a broad diffraction halo centered at $2\theta = 21^\circ$ in X-ray diffraction (XRD) profiles of AUE-3 and AU-3 hydrogels reveals that the amorphous state (Fig. 3C), yet the likely existence of short-range order due to the presence of H-bonding clusters [54]. As presented in the differential scanning calorimetry (DSC) curves with a temperature range of -10-180 °C (Fig. 3D), the absence of melting endothermic peaks of crystalline domains also corroborates the amorphous nature of hydrogels. The glass transition temperatures (Tg) of dry AUE-3 and AU-3 hydrogel films are 122 °C and 116 °C, respectively, and the high Tg values likely stem from strongly UPy-UPy aggregation. Moreover, AUE-3 and AU-3 hydrogel films are highly transparent with the optical transmittance over 82 % in a visible region ranging from 400 to 800 nm (Fig. S11, Supporting **Information**). All these results hint amorphous nature of AUE hydrogel.

Temperature-variable FTIR spectra of the dry AUE-3 hydrogel film from 20 °C to 150 °C were recorded to evaluate the strength and thermal response of hierarchical multiple H-bonding associations. N-H flexural vibration and C=O stretching regions of UPy unit and urethane were investigated emphatically. As represented in Fig. 3E, a variety of interactions forms can be detected mainly with involvement of H-bonds. As the temperature elevates, there are appearing a red-shift corresponding the N-H flexural signal (amide II mode) and blue-shift matching the C=O stretching peak (amide I mode), which are mainly attributed to the disassociation of UPy dimeric and urethane-based H-bonds at high temperature [55]. Meanwhile, the augment of temperature promotes the disassociation of COOH-based H-bonds into free COOH as well, leading to a slightly blue-shift towards higher wavenumbers with the increasing intensity of free COOH. Conclusively, rising temperature would result in weakening of H-bonds. From the energetical perspective, multiple H-bonds may be enthalpy-driven with temperature-induced attenuation effect, implying the translational entropy-driven physical crosslinking interactions [27,56].

2D correlation spectroscopy (2DCOS) analysis based on the temperature-dependent FTIR spectra were further performed to capture more subtle information about internal interaction changes in the representative AUE-3 hydrogel, as shown in Fig. 3F and **G**. In the synchronous map, four main automatic bands at 1714, 1625, 1560 and 1480 cm^{-1} appear, which correspond to the C=O stretching vibration with weak H-bonds in the ester carbonyl group, C=O stretching vibration with strong H-bonds in the amide I band, N-H bending vibration with weak H-bonds in the amide II band and N-H bending vibration with strong H-bonds in the amide II band, respectively. Meanwhile, there are four main cross peaks in the asynchronous map, Φ(1714, 1625), Φ(1714, 1560), Φ(1625, 1560), and Φ(1652, 1480). Based on Noda's judging rule, the responsive order of different groups upon heating is 1714 cm^{-1} → 1560 cm^{-1} → 1625 cm^{-1} → 1480 cm^{-1} (→ means prior to or earlier than). This order highlights that the sequential disassociation of hierarchical multiple H-bonding association within AUE supramolecular network [11,57]. The hierarchical multiple H-bonds are multi-strength with relatively weak H-bonds that can be preferentially dissociated to offer excellent toughness and strongly H-bonds along with hydrophobic-assisting phase separation that help retain the bulk structure of hard domains [58].

To elucidate the packing state of the structure in supramolecular AUE-3 hydrogel, the MD simulations were carried out by creating two simulated systems (AUE-3 and AU-3) [26]. As shown in Fig. 3H and **I**, the average cohesive energy per polymer chains of AUE-3 (378.8 J cm^{-3}) is greater than that of the AU-3 system (303.5 J cm^{-3}), suggesting that a more significant intermolecular interaction in AUE-3 system. One possible explanation is that higher H-bonds interaction density within AUE-3 system, consolidated by the calculated results in which AUE-3 system demonstrates 218 H-bonds, and is higher than that of AU-3 system (150 H-bonds). Furthermore, the binding energies of likely H-bonds between diverse donors and acceptors in AUE-3 hydrogel structures were calculated via DFT simulations (Fig. 3J and Table S2) [26,42]. Obviously, the multiple H-bonds in AUE-3 hydrogel are hierarchical and multi-strength with a strength order of quadruple **>** double **>** single [59], which can efficiently facilitate the acquisition of remarkable integrated properties. In addition, the binding energy of UPy-EGCG is the lowest within various EGCG-based H-bonds, indicating that the crowding of EGCG via H-bonds exerts little impacts on UPy-UPy dimers.

Furthermore, the X-ray photoelectron spectroscopy (XPS) tests were conducted to further investigate the interfacial properties of lyophilized AUE-3 and AU-3 hydrogels. As shown in Fig. 3K, the characteristic peaks of deconvolution C1s spectra in AUE-3 hydrogel are present at 283.8, 284.4, 285.8 and 288.4 eV, originating from C=C (sp^2), C—C (sp^3), C—N/C—O, and C=O, respectively [1]. Simultaneously, the characteristic peaks of deconvolution N1s spectra at 399.9 and 401.7 eV are ascribed to the appearance of NH/N-C=O and N=C, respectively (Fig. 3L). By contrast, the peaks of deconvolution C1s and N1s spectra are identical in AU-3 hydrogel (Fig. S12, Supporting **Information**), except with lower area ratios of C=C and NH/N-C=O, indicating the entrapment of EGCG-based interactions at the interface of AUE-3 hydrogel. This is beneficial to self-aggregation of hydrophobic groups and offering pyrogallol/catechol based binding sites with interfacial interactions for the realization of underwater adhesion.

To further understand the dynamic and reversible property of hierarchical physical crosslinking network in AUE-3 hydrogel, cyclic temperature ramp test by on a rheometer was carried out. As observed in Fig. S13A (Supporting **Information**), both the storage modulus and loss modulus aggrandize gradually, suggesting the transient polymeric network of AUE-3 hydrogel. Remarkably, AUE-3 hydrogel exhibits an opposite viscoelastic transition during the temperature ramp-up process and the ramp curves overlapped well with each other except a slight alternation at low temperature, indicating dynamically viscoelastic behaviors due to the existence of multiple H-bonding cross-links. Likewise, an excellent reversibility was indicated for AU-3 hydrogel as shown in Fig. S13B (Supporting **Information**). Additionally, the tan δ in ramping up curve locates at approximately 7 °C for AUE-3 hydrogel, slightly lower than that of AU-3 hydrogel, and this is likely due to containing the denser quadruple H-bonding crosslinks in AU-3 hydrogel without disturbance of EGCG.

All the above results support that AUE-3 hydrogel network is a phase separation-assisted hierarchical multiple physical crosslinking structure

endowed by supramolecular polymer chain with alkyl hydrophobicity-assisted multiple H-bonds and EGCG-based introduction. This intriguing structure greatly broadens the distribution of the binding strength of physical junctions, exerting a positive effect on reconciling the trade-off between mechanical and adhesive performances. Specifically, the weak H-bonds and random coil PAAc chains contribute to the softness and flexibility, while hydrophobicity-assisted strong H-bonding clusters and phase separation serve as hard domains to achieve high mechanical performances and EGCG-based entrapments promote entropic elasticity and low hysteresis. Remarkably, AUE-3 hydrogel possesses long-lasting and reliable adhesion and excellent anti-swelling outcome, principally resulted from the formation of strong quadruple H-bonds coupled with alkyl-based hydrophobic pockets, and favorable pyrogallol/catechol based binding sites at the interface. Ultimately, by

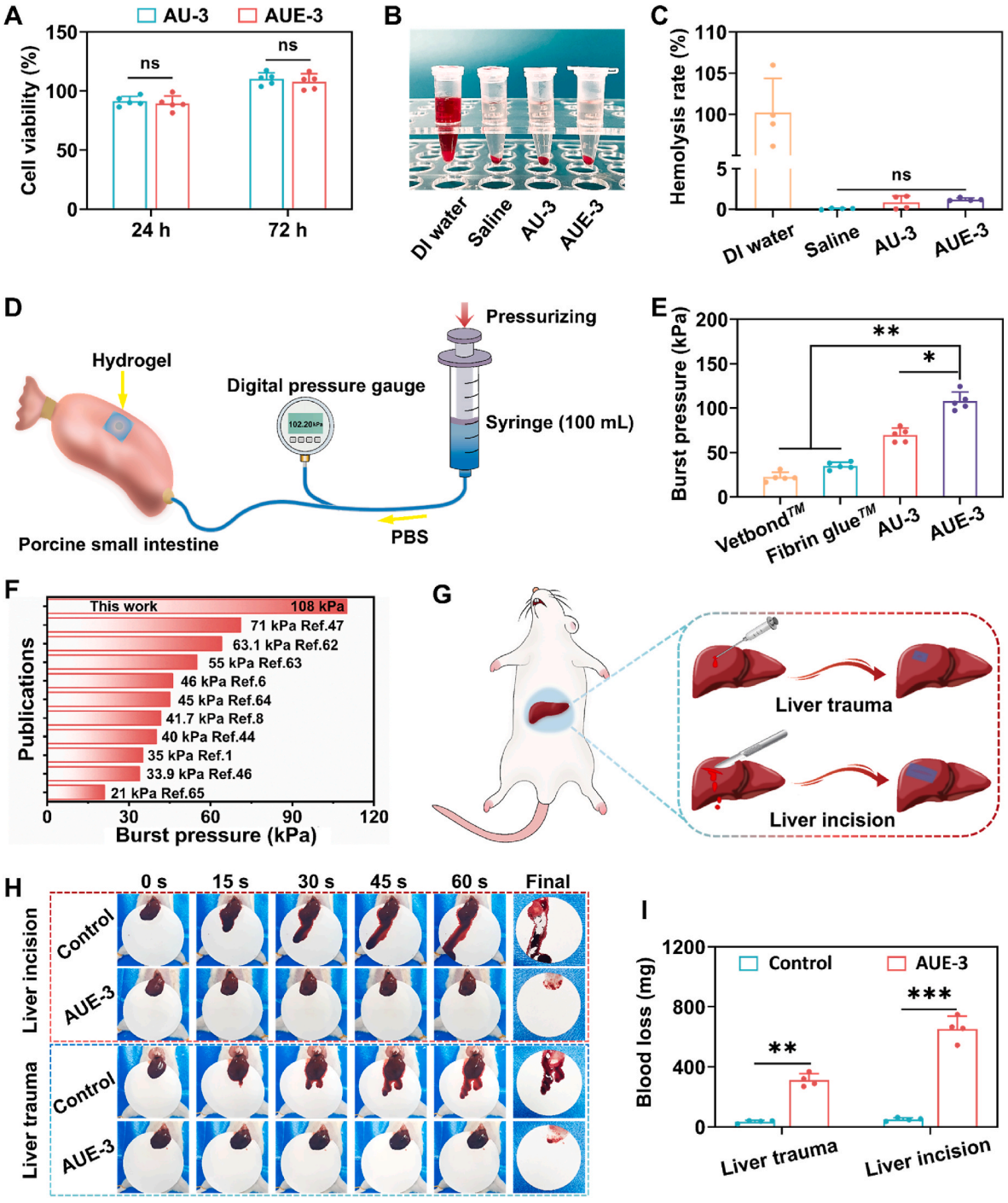

Fig. 4. In vitro biocompatibility and in vivo hemostatic performance of AUE-3 hydrogel. (**A**) Cell viability of L929 cells against AUE-3 hydrogel. (**B**) Hemolysis photographs representing hemolysis phenomenon in different groups. (**C**) Hemolytic rates in different groups. (**D**) Schematic illustration of burst pressure measurement. (**E**) Comparative burst pressure of AUE-3 hydrogel, AU-3 hydrogel and two commercial glues. (**F**) Comparison of burst pressures of this work with recently reported adhesive hydrogels. (**G**) Illustration of protocols for the hemostatic tests on a rat liver trauma model and a rat liver incision model. (**H**) Digital photographs of corresponding bloodstain on filter paper at predetermined time intervals. (**I**) Comparison of blood loss between the AUE-3 group and the control group. Data are expressed as mean ± SD. The significant difference was detected by one-way ANOVA. n = 4 for (**C**, **I**) and n = 5 for (**A**, **E**), $^{*}P < 0.05$, $^{**}P < 0.01$, $^{***}P < 0.001$ and ns: no significance.

leveraging phase separation-assisted hierarchical physical crosslinking junctions with multi-strength, AUE-3 hydrogel is optically transparent, rather-tough, super-stretchable, self-healable, highly adhesive, and water-resistant.

3.5. In vitro biocompatibility and in vivo hemostatic performance of AUE-3 hydrogel

Uncontrollable hemorrhage following trauma or surgery is one of the chief reasons for global mortality, especially for those noncompressible tissue zones, irregularly shaped visceral trauma and high-pressure arteriovenous bleeding are involved [60]. Hence, it is imperative to develop effective hemostatic materials to quickly seal the wounds and achieve hemostasis. It is speculated that AUE-3 hydrogel can act as desirable wound hemorrhaging and closing patch due to its excellent adhesion performance, high mechanical property and promising skin-compliance. Good biocompatibility is the prerequisite for the biomedical applications of AUE-3 hydrogels. As revealed in Fig. 4A, both AUE-3 hydrogel and AU-3 hydrogel (as control) exhibit excellent cytocompatibility witnessed by the high cell viability after incubation for 24 h and 72 h. Besides, the hemocompatibility of the hydrogels was evaluated via in vitro hemolysis assay. As represented in Fig. 4B, the obvious hemoglobin is observed in the supernatant of DI water group after centrifugation, while AU-3 and AUE-3 hydrogels extracts appear almost colorless and transparent, similar to that of saline group, suggesting that the negligible hemolytic effect of AUE-3 hydrogel. Quantitative analysis in Fig. 4C shows that the hemolysis ratios of saline, AU-3 and AUE-3 hydrogels are less than 2 %, confirming a good blood compatibility. Taken together, AUE-3 hydrogel demonstrates outstanding biocompatibility in vitro.

Accounting for the medical application for sealing penetration defects with certain pressure of adhesive patches, the burst pressure tolerance of hydrogel adhesives is a key character [46]. As displayed in Fig. 4D, burst pressure was quantified using a home-designed setup to determine whether AUE-3 hydrogel could form a firm sealing to sustain the flow of PBS inside the porcine small intestine. As shown in Fig. 4E, all hydrogels can seal the wet porcine small intestine filled with PBS without leakage. Compared with two commercially-available tissue sealants (Fibrin sealant and Vetbond) and AU-3 hydrogel, AUE-3 hydrogel demonstrates a significantly stronger wet tissue sealing capacity with the burst pressure reaching as high as 108 ± 9 kPa, remarkably higher than the normal human systolic arterial blood pressure (8–25 kPa) [61]. This superior adhesive property of AUE-3 hydrogel can be ascribed to the excellent balance between cohesive and interfacial adhesion energies of the hydrogel [20,21]. It is also noted that such a super-high burst pressure achieved by AUE-3 hydrogel surpasses recently reported representative adhesive materials (Fig. 4F) [1,6,8,44,46,47,62–65]. Consequently, these results confirm that the AUE-3 hydrogel exhibits an excellent internal tissue sealing capacity, which is particularly advantageous as a promising substitute for sutures and staples in vivo.

Encouraged by its excellent mechanical performances, instant and reliable wet adhesion ability, favorable biocompatibility and outstanding burst pressure capacity, AUE-3 hydrogel was evaluated in vivo as a potential hemostatic patch in liver trauma and liver incision model established in rats (Fig. 4G). The AUE-3 hydrogel was applied to cover the bleeding site during the process of hemostatic and a piece of filter paper was placed under the liver to absorb the blood from the wound to quantify the hemostatic capacity. As represented in Fig. 4H, the blood loss collected by the filter paper on the hemorrhaging sites was recorded. Notably, abundant blood in two models is observed in control group. In stark contrast, the bloodstains in AUE-3 hydrogel group are inconspicuous. Additionally, the quantitative results of the total blood loss both in two models were illustrated in Fig. 4I. Consistent with the above intuitive results, the control groups exhibit severe blood loss of 312 ± 37.3 mg in the liver trauma model and 653 ± 72.6 mg in the liver incision model, while the total blood losses in AUE-3 group are dramatically reduced to 35 ± 7.6 mg and 50 ± 8.7 mg, respectively, indicating the superb hemostatic ability of AUE-3 hydrogel. Probably, this efficient hemostatic performance in vivo can be derived from its rapid and tough adhesion capacity of AUE-3 hydrogel and blood coagulation supported by EGCG, making it serving as a user-friendly physical barrier to stop bleeding [4]. In conclusion, the data demonstrate its prospect in utilization for self-rescue in emergency situations.

3.6. In vitro antioxidant capability, antibacterial properties and in vivo wound closure performance of AUE-3 hydrogel

Typically, excessive reactive oxygen species and bacterial infection have been considerable obstacles that hinder wound healing during a surgical procedure [22]. Hence, adhesive hydrogel patches with antioxidant and antimicrobial functions are crucial to the accomplishment of accelerating wound closure and repair. Previous reports pointed out that EGCG, the most abundant and bioactive compound of green tea extract, is of interest with respect to retarding oxidative stress and controlling microbial spoilage [66]. Consequently, the antioxidant effect of AUE-3 hydrogel was determined via a DPPH radical scavenging assay, ABTS radical scavenging assay and PTIO radical scavenging assay based on the previous protocol [25,66,67]. As revealed in Fig. 5A and Fig. S14A (Supporting **Information**), AUE-3 hydrogel represents a desirable DDPH clearance efficiency as high as 88.5 ± 1.7 % after 5 min incubation, while that of AU-3 hydrogel merely sustains at 4.2 ± 1.5 %. Compared with control and AU-3 groups, the color in AUE-3 group intuitively turns yellow in Fig. 5B, further suggesting that AUE-3 hydrogel can efficiently eliminate free radicals. In addition, as shown in Figs. S14B and C, AUE-3 hydrogel can eliminate almost all ABTS radicals with scavenging efficiency as high as 97.9 ± 1.5 % after 5 min incubation, while AU-3 hydrogel can merely clear 2.6 ± 1.4 % ABTS radicals. Similarly, compared with AU-3 hydrogel with 1.1 ± 0.3 % PTIO scavenging activity, AUE-3 hydrogel also exhibits an excellent PTIO clearance efficiency and can achieve 79.5 ± 2.1 % PTIO scavenging activity after 4 h incubation (Figs. S14D and E). These results directly mirror that EGCG-based polyphenols play a key role in excellent antioxidant capacity of AUE-3 hydrogel.

It has been demonstrated above that AUE-3 hydrogel possesses excellent antioxidant capacity. To further determine whether AUE-3 hydrogel can protect cell from oxidative stress damage, the cytotoxicity of AUE-3 hydrogel in the presence of H_2O_2 was determined by CCK-8 assay. As illustrated in Fig. S15 (Supporting **Information**), the viability of unprotected cells (H_2O_2 group) and cells treated with AU-3 hydrogel (AU-3 + H_2O_2 group) were only 63.1 ± 13.0 % and 61.6 ± 11.6 % under oxidative stress conditions, while that of H_2O_2-treated cells protected by AUE-3 hydrogel (AUE-3 + H_2O_2 group) was significantly increased to 91.4 ± 5.9 %, indicating that AUE-3 hydrogel can effectively protect L929 cells against H_2O_2-induced oxidative stress injury and reduce cell apoptosis caused by pathological oxidative stress [68].

Subsequently, the antibacterial activity of AUE-3 hydrogel was evaluated by selecting *Escherichia coli* (*E. coli*) and *Staphylococcus aureus* (*S. aureus*) as typical Gram-negative and Gram-positive bacteria, respectively. As shown in Fig. S16A (Supporting **Information**), the antibacterial efficiencies of AUE-3 hydrogel are enhanced with the increasing of AUE-3 hydrogel content, and 0.3 g mL^{-1} is determined as MIC90. Then, in vitro antibacterial activities of AUE-3 hydrogel at MIC90 were further investigated in Fig. 5C, and the bacteria treated by PBS was chosen as control group. Obviously, for control and AU-3 groups, the bacterial survival rates for both *E. coli* and *S. aureus* are over 90 %, indicating a negligible antibacterial activity of AU-3 hydrogel. In comparison, AUE-3 hydrogel exhibits excellent antibacterial activities against both *E. coli* and *S. aureus* with significantly lower bacterial survival rates. Meanwhile, AUE-3 hydrogel demonstrates of the distinct inhibition circles on both *E. coli* and *S. aureus* for 12 h co-

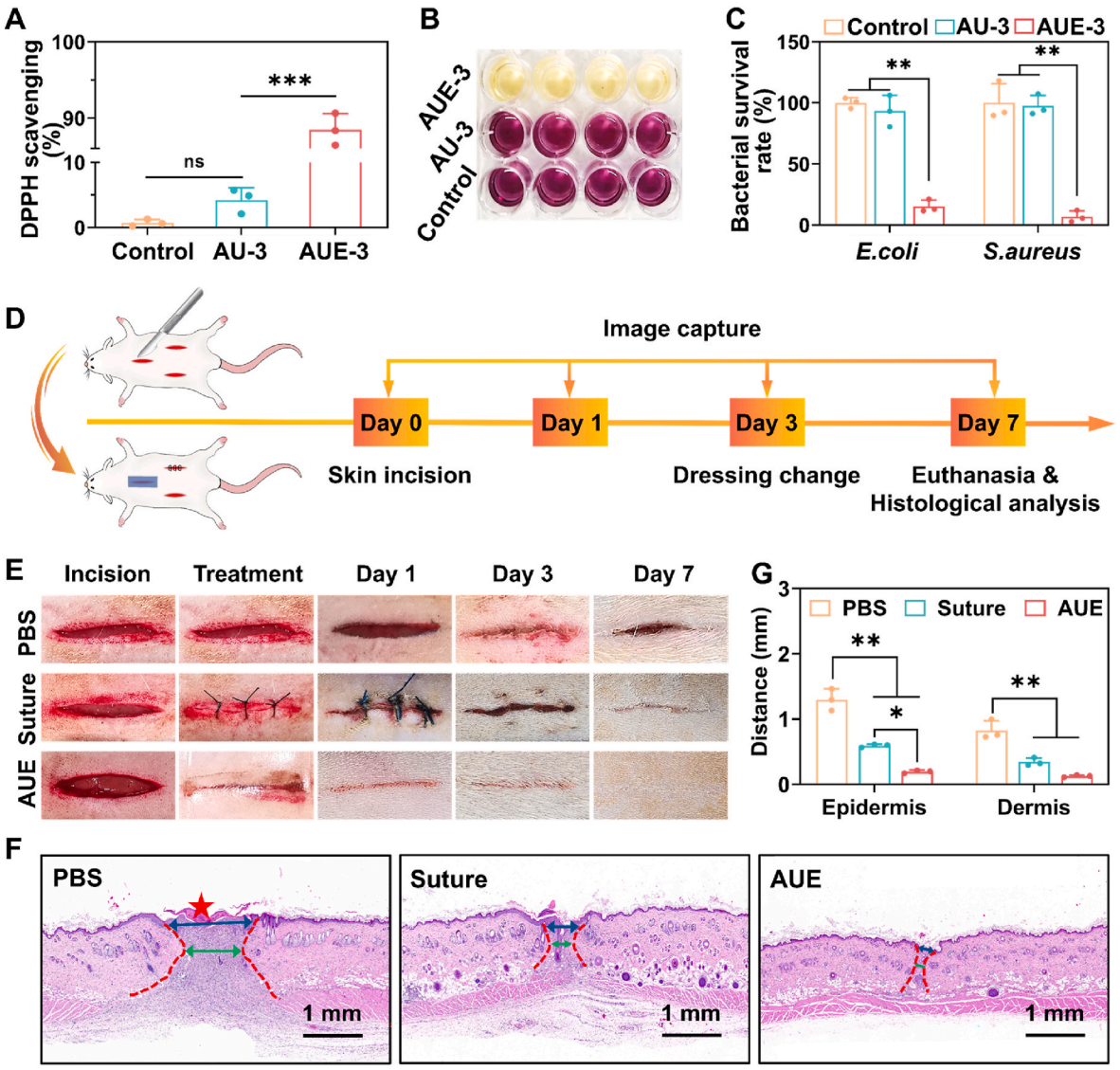

Fig. 5. In vitro antioxidant capability, antibacterial properties and in vivo wound closure performance of AUE-3 hydrogel. (**A**) DPPH scavenging efficiency ofAUE-3 hydrogel after 5 min incubation. (**B**) Digital photograph of DPPH solution treated with AUE-3 hydrogel after 5 min incubation. (**C**) Bacterial survival rates of the AUE-3 hydrogel against *E. coli* and *S. aureus*. (**D**) Schematic illustration of the establishment skin incision wounds treated by AUE-3 hydrogel. (**E**) Representative photographs of wound healing at various time intervals after treatment with PBS, suture and AUE-3 hydrogel, respectively. (**F**) H&E staining of the wound sections after 7 days. The blue arrows represent the length of the epidermis defect, and the green arrows demonstrate the length of the dermis defect. Scale bar: 1 mm. (**G**) Statistical wound lengths of the epidermis and dermis after treatment for 7 days. Data are expressed as mean ± SD. The significant difference was detected by one-way ANOVA. n = 3 for (**A**, **C**, **G**), $^{*}P < 0.05$, $^{**}P < 0.01$, $^{***}P < 0.001$ and ns: no significance.

culturing, while AU-3 hydrogel does not (Fig. S16B, Supporting **Information**). The above results confirm that AUE-3 hydrogel owns outstanding bacteria inhibiting performance, presumably due to the EGCG molecules released from the AUE-3 hydrogel that damage the cell walls of *S. aureus* and *E. coli* via binding to the peptidoglycan layer and producing hydrogen peroxide, respectively [69,70]. Above all, AUE-3 hydrogel shows efficient antioxidant activity and bacteria inhibiting capacity imparted by bioactive EGCG.

The above results demonstrating the strengthening and stiffening effects of the AUE-3 hydrogel by leveraging HMHHS portent its application as new adhesive patches, and its inherent biocompatibility, hemostatic property, antioxidant capacity and antibacterial property also hold great importance for protecting adhesion in emergencies. Hence, a full-thickness rat skin incision model (male, incision length = 2 cm) was used to further investigate the practical wound closure and healing effects of the AUE-3 hydrogel as a band-aid on the moving parts. As shown in Fig. 5D, the cut AUE-3 hydrogel strip was applied to the incision (AUE group) and replaced by a new one on day 3 post-operation to mimic dressing change clinically, while surgical suture (suture group) and merely sterile PBS washing (PBS group) were used as positive and negative controls, respectively. The wound closure process was observed with a digital camera on day 1, 3 and 7 after operation.

AUE-3 hydrogel can successfully close the wounds within 2 min and maintains wound closure resisting the tensile force of the skin during the healing process. Meanwhile, the excellent transparent feature of AUE-3 hydrogel is capable to facilitate the observation of the wound condition and avoiding secondary injury. Fig. 5E displays the wound incisions gradually vanishing process from day 1 to day 7 and ultimately smooth and neat wound closure surface with negligible scarring formation on day 7 in AUE-3 hydrogel-treated group. However, the PBS-treated group shows failed wound closure with obvious blood crusts and scars, and the delayed closure condition coupled with apparent scars and secondary injury is seen in suture-treated group. The final wound closure rate reaches 96 % in AUE group whilst those of the suture group and PBS

group are 65 % and 47 %, respectively (Fig. S17, Supporting **Information**).

Histological results of the tissue regeneration in the defected skin on day 7 were further visualized by H&E staining and immunofluorescent (IF) staining. As demonstrated in Fig. 5F, an intact epidermis layer appears in the AUE group, indicating realizing complete epidermal regeneration, whereas the PBS group fails with evident scars observed on the top (red star) and fibrous tissue disorder, and the sutured group shows unregenerated glandular cavity, possible intercellular edema and secondary wound caused by the suture needle even though the seemingly intact epidermal layer. Further, compared with other groups with a number of inflammatory cells observed at the incision sites, AUE group demonstrates no apparent inflammation and almost absent gap between the dermis incision edges, suggesting a much better tissue regeneration, which presumably results from the antioxidant capacity of the AUE-3 hydrogel endowed by bioactive EGCG [22]. IF staining of CD68 further demonstrates that significantly higher levels of macrophage recruitment in the wound areas for both PBS group and suture group compared with a more subdued inflammatory status for AUE group on day 7 (Fig. S18, Supporting **Information**), indicating that AUE-3 hydrogel can accelerate the wound repair by alleviating inflammation at the wound site [6]. In addition, Fig. 5G provided the quantization results of the lengths of premature tissues including the epidermis and dermis. Significantly, the shortest lengths both in the epidermis and dermis are observed in AUE group. After 7 days, the length of the dermis markedly decreases to 0.1 mm in AUE group compared with higher values in PBS and suture group (0.8 and 0.4 mm, respectively). In conclusion, these results demonstrate that the AUE group exhibits the best wound closure and repair effect.

Furthermore, collagen deposition provides the matrix for restoring tissue structure and function during wound healing [25]. As shown in Masson's trichrome staining results of Fig. S18 (Supporting **Information**), the collagen deposition (blue) level of AUE group is significantly higher than those of other two groups on day 7, confirming the improved extracellular matrix reconstruction and tissue remodeling for incision sites treated by AUE-3 hydrogel. Combined with above histological assessments, AUE-3 hydrogel can facilitate wound healing by achieving rapid wound closure, reducing inflammation and accelerating collagen deposition.

Profitably, AUE-3 hydrogel with excellent adhesive capacity can effectively achieve rapid and reliable wound closure, minimizing wound exudating and keeping the wound clean continuously, thereby avoiding bacterial infection. More significantly, AUE-3 hydrogel offers a suitable mechanical support for wound healing, assisting tissue regeneration and preventing scars formation. Additionally, the transparency facilitates the observation of wound closure and repair process, enabling timely managements. The good flexibility and conformability of the hydrogel also contribute to deforming or stretching following the moving parts, avoiding detachment from the moving surface. Overall, AUE-3 hydrogels with good biocompatibility, superior tissue adhesion performance and suitable mechanical support have shown promising application in the clinical translation as tissue adhesive patches.

4. Conclusions

In this work, we have reported a supramolecular hydrogel patch by in situ copolymerization of a liquid-liquid phase separation precursor and the incorporation of bioactive EGCG. It is highlighted that the resultant AUE hydrogel leverages hierarchical multi-strength H-bonds hinged strategy to broaden the distribution of the binding strength of physical junctions, facilitating the acquisition of remarkable properties. More intriguingly, a canonical balance between superb mechanical performance and robust adhesive capacity can be achieved. On the one hand, the synergistic effect of multi-strength H-bonds is capable of serving as crosslinkers and reinforcing hard domains simultaneously to enhance mechanical performances. On the other hand, rigid UPy motifs assisted by alkyl-based hydrophobic pockets and the entrapment of EGCG are promotional for anti-swelling behavior and underwater adhesion. The dynamic characteristics of noncovalent crosslinks are utilized to guarantee self-healing behavior, viscoelasticity and reversible adhesiveness. In addition, the crowding of EGCG confer the hydrogel with the entropy-based elasticity, accompanying surprising biological properties. The high burst pressure tolerance, rapid hemorrhage control and effective wound closure are further demonstrated in AUE-3 hydrogel, providing an insight for biomedical applications as self-rescue tissue adhesives with high operability. Overall, the strategy used in this report is comparably universal and can be used to realize programmable mechanical and adhesive performances to further widen applicable platforms.

Ethics approval and consent to participate

All the protocols for animal care and experiments procedures were conducted in accordance with the guidelines of the Council for the Purpose of Control and Supervision of Experiments on Animals, Ministry of Public Health, China. The animal protocols were approved by the Institutional Animal Care and Use Committee of Yi Shengyuan Gene Technology (Tianjin) Co. Ltd (Approval No. YSY-DWLL-2023374 and YSY-DWLL-2023375 for Sprague-Durer rats).

CRediT authorship contribution statement

Jumin Yang: Writing – original draft, Visualization, Software, Formal analysis, Data curation, Conceptualization. **Wenguang Liu:** Writing – review & editing, Methodology, Conceptualization. **Wei Wang:** Writing – review & editing, Formal analysis, Conceptualization.

Declaration of competing interest

The authors declare no conflict of interest.

Acknowledgements

This work was supported by National Key Research and Development Program of China (No. 2021YFE0105400) and the National Natural Science Foundation of China grant (No. 32371404).

Appendix A. Supplementary data

Supplementary data to this article can be found online at https://doi.org/10.1016/j.bioactmat.2024.09.014.

References

[1] J. Yu, R. Xie, M. Zhang, K. Shen, Y. Yang, X. Zhao, X. Zhang, Y. Zhang, Y. Cheng, Molecular architecture regulation for the design of instant and robust underwater adhesives, Sci. Adv. 9 (2023) eadg4031.
[2] N. Li, Y. Li, Z. Cheng, Y. Liu, Y. Dai, S. Kang, S. Li, N. Shan, S. Wai, A. Ziaja, Y. Wang, J. Strzalka, W. Liu, C. Zhang, X. Gu, J.A. Hubbell, B. Tian, S. Wang, Bioadhesive polymer semiconductors and transistors for intimate biointerfaces, Science 381 (2023) 686–693.
[3] J. Yu, Y. Qin, Y. Yang, X. Zhao, Z. Zhang, Q. Zhang, Y. Su, Y. Zhang, Y. Cheng, Robust hydrogel adhesives for emergency rescue and gastric perforation repair, Bioact. Mater. 19 (2023) 703–716.
[4] L. Wang, L. Duan, G. Liu, J. Sun, M.A. Shahbazi, S.C. Kundu, R.L. Reis, B. Xiao, X. Yang, Bioinspired polyacrylic acid-based dressing: wet adhesive, self-healing, and multi-biofunctional coacervate hydrogel accelerates wound healing, Adv. Sci. 10 (2023) 2207352.
[5] X. Wang, Y. Guo, J. Li, M. You, Y. Yu, J. Yang, G. Qin, Q. Chen, Tough wet adhesion of hydrogen-bond-based hydrogel with on-demand debonding and efficient hemostasis, ACS Appl. Mater. Interfaces 14 (2022) 36166–36177.
[6] H. Ren, Z. Zhang, X. Cheng, Z. Zou, X. Chen, C. He, Injectable, self-healing hydrogel adhesives with firm tissue adhesion and on-demand biodegradation for sutureless wound closure, Sci. Adv. 9 (2023) eadh4327.
[7] Y. Li, G. Li, Y. Chen, X. Zhao, Y. Wang, J. Liu, Z. Li, Gradient modulus tissue adhesive composite for dynamic wound closure, Adv. Funct. Mater. 32 (2022) 2207306.

[8] W. Peng, C. Liu, Y. Lai, Y. Wang, P. Liu, J. Shen, An adhesive/anti-adhesive Janus tissue patch for efficient closure of bleeding tissue with inhibited postoperative adhesion, Adv. Sci. 10 (2023) 2301427.

[9] Y. Wei, Y. He, C. Wang, G. Chen, B. Zhao, Asymmetric "Janus" biogel for human-machine interfaces, Adv. Funct. Mater. 33 (2023) 2214366.

[10] H. Wang, X. Yi, T. Liu, J. Liu, Q. Wu, Y. Ding, Z. Liu, Q. Wang, An integrally formed Janus hydrogel for robust wet-tissue adhesive and anti-postoperative adhesion, Adv. Mater. 35 (2023) 2300394.

[11] H. Ye, B. Wu, S. Sun, P. Wu, Self-compliant ionic skin by leveraging hierarchical hydrogen bond association, Nat. Commun. 15 (2024) 885.

[12] C. Chen, Y. Wang, H. Zhang, H. Zhang, W. Dong, W. Sun, Y. Zhao, Responsive and self-healing structural color supramolecular hydrogel patch for diabetic wound treatment, Bioact. Mater. 15 (2022) 194–202.

[13] Y. Li, C. Zhu, Y. Dong, D. Liu, Supramolecular hydrogels: mechanical strengthening with dynamics, Polymer 210 (2020) 122993.

[14] L. Voorhaar, R. Hoogenboom, Supramolecular polymer networks: hydrogels and bulk materials, Chem. Soc. Rev. 45 (2016) 4013–4031.

[15] R.P. Sijbesma, F.H. Beijer, L. Brunsveld, B.J. Folmer, J.H. Hirschberg, F.M. Lange, J.K. Lowe, E.W. Meijer, Reversible polymers formed from self-complementary monomers using quadruple hydrogen bonding, Science 278 (1997) 1601–1604.

[16] I. Jeon, J. Cui, W.R.K. Illeperuma, J. Aizenberg, J.J. Vlassak, Extremely stretchable and fast self-healing hydrogels, Adv. Mater. 28 (2016) 4678–4683.

[17] X. Chang, Y. Geng, H. Cao, J. Zhou, Y. Tian, G. Shan, Y. Bao, Z.L. Wu, P. Pan, Dual-crosslink physical hydrogels with high toughness based on synergistic hydrogen bonding and hydrophobic interactions, Macromol. Rapid Commun. 39 (2018) 1700806.

[18] X. Liu, Q. Zhang, G. Gao, Solvent-resistant and nonswellable hydrogel conductor toward mechanical perception in diverse liquid media, ACS Nano 14 (2020) 13709–13717.

[19] C. Yuan, M. Yang, X. Ren, Q. Zou, X. Yan, Porphyrin/ionic-liquid co-assembly polymorphism controlled by liquid–liquid phase separation, Angew. Chem., Int. Ed. 59 (2020) 17456–17460.

[20] K. Liu, P. Wu, Small ionic-liquid-based molecule drives strong adhesives, Angew. Chem., Int. Ed. 63 (2024) e202403220.

[21] J. Xiong, M. Duan, X. Zou, S. Gao, J. Guo, X. Wang, Q. Li, W. Li, X. Wang, F. Yan, Biocompatible tough ionogels with reversible supramolecular adhesion, J. Am. Chem. Soc. 146 (2024) 13903–13913.

[22] Z. Yuan, X. Duan, X. Su, Z. Tian, A. Jiang, Z. Wan, H. Wang, P. Wei, B. Zhao, X. Liu, J. Huang, Catch bond-inspired hydrogels with repeatable and loading rate-sensitive specific adhesion, Bioact. Mater. 21 (2023) 566–575.

[23] H. Fu, J. Huang, J.J.B. van der Tol, L. Su, Y. Wang, S. Dey, P. Zijlstra, G. Fytas, G. Vantomme, P.Y.W. Dankers, E.W. Meijer, Supramolecular polymers form tactoids through liquid–liquid phase separation, Nature 626 (2024) 1011–1018.

[24] T. Liu, F. Wang, Q. Wu, T. Chen, P. Sun, Fluorescent, electrically responsive and ultratough self-healing hydrogels via bioinspired all-in-one hierarchical micelles, Mater. Horiz. 8 (2021) 3096–3104.

[25] J. Yang, X. Jin, W. Liu, W. Wang, A programmable oxygenation device facilitates oxygen generation and replenishment to promote wound healing, Adv. Mater. 35 (2023) 2305819.

[26] C. Wang, X. Geng, J. Chen, H. Wang, Z. Wei, B. Huang, W. Liu, X. Wu, L. Hu, G. Su, J. Lei, Z. Liu, X. He, Multiple H-bonding cross-linked supramolecular solid–solid phase change materials for thermal energy storage and management, Adv. Mater. 36 (2023) 2309723.

[27] W. Zhang, B. Wu, S. Sun, P. Wu, Skin-like mechanoresponsive self-healing ionic elastomer from supramolecular zwitterionic network, Nat. Commun. 12 (2021) 4082.

[28] L. Su, J. Mosquera, M.F.J. Mabesoone, S.M.C. Schoenmakers, C. Muller, M.E. J. Vleugels, S. Dhiman, S. Wijker, A.R.A. Palmans, E.W. Meijer, Dilution-induced gel-sol-gel-sol transitions by competitive supramolecular pathways in water, Science 377 (2022) 213–218.

[29] C. Cui, C. Fan, Y. Wu, M. Xiao, T. Wu, D. Zhang, X. Chen, B. Liu, Z. Xu, B. Qu, W. Liu, Water-triggered hyperbranched polymer universal adhesives: from strong underwater adhesion to rapid sealing hemostasis, Adv. Mater. 31 (2019) 1905761.

[30] B. Zhang, Y. Qin, L. Yang, Y. Wu, N. Chen, M. Li, Y. Li, H. Wan, D. Fu, R. Luo, L. Yuan, Y. Wang, A polyphenol-network-mediated coating modulates inflammation and vascular healing on vascular stents, ACS Nano 16 (2022) 6585–6597.

[31] J. Wang, B. Wu, P. Wei, S. Sun, P. Wu, Fatigue-free artificial ionic skin toughened by self-healable elastic nanomesh, Nat. Commun. 13 (2022) 4411.

[32] S. Datta, M.L. Saha, P.J. Stang, Hierarchical assemblies of supramolecular coordination complexes, Accounts Chem. Res. 51 (2018) 2047–2063.

[33] D. Zhalmuratova, T.G. La, K.T. Yu, A.R.A. Szojka, S.H.J. Andrews, A.B. Adesida, C. I. Kim, D.S. Nobes, D.H. Freed, H.J. Chung, Mimicking "J-shaped" and anisotropic stress–strain behavior of human and porcine aorta by fabric-reinforced elastomer composites, ACS Appl. Mater. Interfaces 11 (2019) 33323–33335.

[34] J. Xiong, X. Wang, L. Li, Q. Li, S. Zheng, Z. Liu, W. Li, F. Yan, Low-hysteresis and high-toughness hydrogels regulated by porous cationic polymers: the effect of counteranions, Angew. Chem., Int. Ed. 63 (2023) e202316375.

[35] R. Zhu, D. Zhu, Z. Zheng, X. Wang, Tough double network hydrogels with rapid self-reinforcement and low hysteresis based on highly entangled networks, Nat. Commun. 15 (2024) 1344.

[36] Y. Song, Y. Liu, T. Qi, G.L. Li, Towards dynamic but supertough healable polymers through biomimetic hierarchical hydrogen-bonding interactions, Angew. Chem., Int. Ed. 57 (2018) 13838–13842.

[37] J. Wang, F. Tang, C. Yao, L. Li, Low hysteresis hydrogel induced by spatial confinement, Adv. Funct. Mater. 33 (2023) 2214935.

[38] J. Zou, X. Jing, Z. Chen, S.J. Wang, X.S. Hu, P.Y. Feng, Y.J. Liu, Multifunctional organohydrogel with ultralow-hysteresis, ultrafast-response, and whole-strain-range linearity for self-powered sensors, Adv. Funct. Mater. 33 (2023) 2213895.

[39] S. Guan, C. Xu, X. Dong, M. Qi, A highly tough, fatigue-resistant, low hysteresis hybrid hydrogel with a hierarchical cross-linked structure for wearable strain sensors, J. Mater. Chem. A 11 (2023) 15404–15415.

[40] M. Hua, S. Wu, Y. Ma, Y. Zhao, Z. Chen, I. Frenkel, J. Strzalka, H. Zhou, X. Zhu, X. He, Strong tough hydrogels via the synergy of freeze-casting and salting out, Nature 590 (2021) 594–599.

[41] X. Li, K. Cui, Y. Zheng, Y.N. Ye, C. Yu, W. Yang, T. Nakajima, J.P. Gong, Role of hierarchy structure on the mechanical adaptation of self-healing hydrogels under cyclic stretching, Sci. Adv. 9 (2023) eadj6856.

[42] K. Yang, Q. Li, S. Tian, J. Wang, G. Lu, H. Guo, S. Xu, L. Zhang, J. Yang, Highly stretchable, self-healing, and sensitive e-skins at −78 °C for polar exploration, J. Am. Chem. Soc. 146 (2024) 10699–10707.

[43] X. Ni, Z. Yang, J. Li, Scaling behavior of fracture properties of tough adhesive hydrogels, ACS Macro Lett. 10 (2021) 180–185.

[44] K. Chen, C. Liu, J. Huang, L. Che, Y. Yuan, C. Liu, A conformable and tough Janus adhesive patch with limited 1D swelling behavior for internal bioadhesion, Adv. Funct. Mater. 33 (2023) 2303836.

[45] W. Xue, R. Yang, S. Liu, Y. Pu, P. Wang, W. Zhang, X. Tan, B. Chi, Ascidian-inspired aciduric hydrogels with high stretchability and adhesiveness promote gastric hemostasis and wound healing, Biomater. Sci. 10 (2022) 2417–2427.

[46] X. Chen, J. Zhang, G. Chen, Y. Xue, J. Zhang, X. Liang, I.M. Lei, J. Lin, B.B. Xu, J. Liu, Hydrogel bioadhesives with extreme acid-tolerance for gastric perforation repairing, Adv. Funct. Mater. 32 (2022) 2202285.

[47] P. Ma, W. Liang, R. Huang, B. Zheng, K. Feng, W. He, Z. Huang, H. Shen, H. Wang, D. Wu, Super-structured wet-adhesive hydrogel with ultralow swelling, ultrahigh burst pressure tolerance, and anti-postoperative adhesion properties for tissue adhesion, Adv. Mater. 36 (2023) 2305400.

[48] W. Zhang, R. Wang, Z. Sun, X. Zhu, Q. Zhao, T. Zhang, A. Cholewinski, F. Yang, B. Zhao, R. Pinnaratip, P.K. Forooshani, B.P. Lee, Catechol-functionalized hydrogels: biomimetic design, adhesion mechanism, and biomedical applications, Chem. Soc. Rev. 49 (2020) 433–464.

[49] W. Li, X. Liu, Z. Deng, Y. Chen, Q. Yu, W. Tang, T.L. Sun, Y.S. Zhang, K. Yue, Tough bonding, on-demand debonding, and facile rebonding between hydrogels and diverse metal surfaces, Adv. Mater. 31 (2019) 1904732.

[50] K. Li, X. Zan, C. Tang, Z. Liu, J. Fan, G. Qin, J. Yang, W. Cui, L. Zhu, Q. Chen, Tough, instant, and repeatable adhesion of self-healable elastomers to diverse soft and hard surfaces, Adv. Sci. 9 (2022) 2105742.

[51] R. Michel, L. Poirier, Q. Poelvoorde, J. Legagneux, M. Manassero, L. Corté, Interfacial fluid transport is a key to hydrogel bioadhesion, Proc. Natl. Acad. Sci. U. S.A. 116 (2019) 738–743.

[52] G.M. Taboada, K. Yang, M.J.N. Pereira, S.S. Liu, Y. Hu, J.M. Karp, N. Artzi, Y. Lee, Overcoming the translational barriers of tissue adhesives, Nat. Rev. Mater. 5 (2020) 310–329.

[53] M. Doi, Onsager principle in polymer dynamics, Prog. Polym. Sci. 112 (2021).

[54] Y. Shi, B. Wu, S. Sun, P. Wu, Aqueous spinning of robust, self-healable, and crack-resistant hydrogel microfibers enabled by hydrogen bond nanoconfinement, Nat. Commun. 14 (2023) 1370.

[55] J. Joseph, E.D. Jemmis, Red-, blue-, or no-shift in hydrogen bonds: a unified explanation, J. Am. Chem. Soc. 129 (2007) 4620–4632.

[56] C.A. Yu, H. Lian, X. Kong, L.H. Hector, J. Qin, A.E. Appel, Physical networks from entropy-driven non-covalent interactions, Nat. Commun. 12 (2021) 746.

[57] H. Wan, B. Wu, L. Hou, P. Wu, Amphibious polymer materials with high strength and superb toughness in various aquatic and atmospheric environments, Adv. Mater. 36 (2023) 2307290.

[58] D. Wang, J. Xu, J. Chen, P. Hu, Y. Wang, W. Jiang, J. Fu, Transparent, mechanically strong, extremely tough, self-recoverable, healable supramolecular elastomers facilely fabricated via dynamic hard domains design for multifunctional applications, Adv. Funct. Mater. 30 (2019) 1907109.

[59] Y. Song, Y. Liu, T. Qi, G.L. Li, Towards dynamic but supertough healable polymers through biomimetic hierarchical hydrogen-bonding interactions, Angew. Chem. Int. Ed. 57 (2018) 13838–13842.

[60] Y. Hong, F. Zhou, Y. Hua, X. Zhang, C. Ni, D. Pan, Y. Zhang, D. Jiang, L. Yang, Q. Lin, Y. Zou, D. Yu, D.E. Arnot, X. Zou, L. Zhu, S. Zhang, H. Ouyang, A strongly adhesive hemostatic hydrogel for the repair of arterial and heart bleeds, Nat. Commun. 10 (2019) 2060.

[61] K.A. Vakalopoulos, F. Daams, Z. Wu, L. Timmermans, J.J. Jeekel, G.-J. Kleinrensink, A. van der Ham, J.F. Lange, Tissue adhesives in gastrointestinal anastomosis: a systematic review, J. Surg. Res. 180 (2013) 290–300.

[62] E. Shirzaei Sani, A. Kheirkhah, D. Rana, Z. Sun, W. Foulsham, A. Sheikhi, A. Khademhosseini, R. Dana, N. Annabi, Sutureless repair of corneal injuries using naturally derived bioadhesive hydrogels, Sci. Adv. 5 (2019) eaav1281.

[63] H. Wang, J. Cheng, F. Sun, X. Dou, J. Liu, Y. Wang, M. Li, J. Gao, X. Liu, X. Wang, F. Yang, Z. Zhu, H. Shen, L. Zhang, P. Tang, D. Wu, A super tough, rapidly biodegradable, ultrafast hemostatic bioglue, Adv. Mater. 35 (2023) 2208622.

[64] J. Wu, H. Yuk, L.T. Sarrafian, C. Guo, G.L. Griffiths, S.C. Nabzdyk, X. Zhao, An off-the-shelf bioadhesive patch for sutureless repair of gastrointestinal defects, Sci. Transl. Med. 14 (2022) eabh2857.

[65] W. Yang, C. Xuan, X. Liu, Q. Zhang, K. Wu, L. Bian, X. Shi, A sandwiched patch toward leakage-free and anti-postoperative tissue adhesion sealing of intestinal injuries, Bioact. Mater. 24 (2023) 112–123.

[66] S. Lee, J. Lee, H. Byun, S. Kim, J. Joo, H.H. Park, H. shin, Evaluation of the anti-oxidative and ROS scavenging properties of biomaterials coated with

epigallocatechin gallate for tissue engineering, Acta Biomater. 124 (2021) 166–178.
[67] X. Li, 2-Phenyl-4,4,5,5-tetramethylimidazoline-1-oxyl 3-oxide (PTIO•) radical scavenging: a new and simple antioxidant assay in vitro, J. Agric. Food Chem. 65 (2017) 6288–6297.
[68] Y. Guan, H. Niu, Z. Liu, Y. Dang, J. Shen, M. Zayed, L. Ma, J. Guan, Sustained oxygenation accelerates diabetic wound healing by promoting epithelialization and angiogenesis and decreasing inflammation, Sci. Adv. 7 (2021) eabj0153.
[69] M. Nikoo, J.M. Regenstein, H.A. Gavlighi, Antioxidant and antimicrobial activities of (-)-epigallocatechin-3-gallate (EGCG) and its potential to preserve the quality and safety of foods, Compr. Rev. Food Sci. Food Saf. 17 (2018) 732–753.
[70] R. Hengge, Targeting bacterial biofilms by the green tea polyphenol EGCG, Molecules 24 (2019) 2403.